

Master's thesis

2019

Master's thesis

Gudrun Glende

NTNU
Norwegian University of
Science and Technology
Faculty of Natural Sciences
Department of Materials Science and Engineering

Gudrun Glende

Molecular Dynamics Simulations of Antagonistic Salt at the Water/Oil Interface

July 2019



Norwegian University of
Science and Technology

Molecular Dynamics Simulations of Antagonistic Salt at the Water/Oil Interface

Gudrun Glende

Materials Science and Engineering

Submission date: July 2019

Supervisor: Astrid S. de Wijn

Co-supervisor: Faezeh Pousaneh

Norwegian University of Science and Technology
Department of Materials Science and Engineering

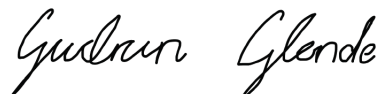
Preface

This thesis represent the work and results associated with the final master's thesis at the Department of Mechanical Engineering at Norwegian University of Science and Technology, Trondheim. This master's thesis is the final part of my Master of Science in Materials Science and Engineering.

The work with this thesis started with the pre-master's thesis, which lasted from August 30, 2018 til January 8, 2019, and ended with the master's thesis, which lasted from January 15, 2019 until it was delivered July 8, 2019.

The work was done by Gudrun Glende with support from supervisor Astrid de Wijn and co-supervisor Faezeh Pousaneh. I want to thank you both for all your guidance and support throughout the pre-master's and master's thesis.

Trondheim, July 8, 2019

A handwritten signature in black ink that reads "Gudrun Glende". The script is cursive and fluid, with the first letters of "Gudrun" and "Glende" being capitalized and prominent.

Gudrun Glende

Abstract

Mixtures composed of water and organic solvents are very common. They are found inside our bodies and in many industries. A mixture composed of water and the organic solvent 2,6-lutidine is a uniform mixture at higher and lower temperatures. In the mid region the mixture will separate into two phases, water and organic, and form a two-phase region. This thesis has studied the variation of tension between the two phases when an antagonistic salt is introduced.

An antagonistic salt is a salt composed of a hydrophilic and a hydrophobic part. The hydrophilic part is attracted to water, and dissolves in the water phase. The hydrophobic part is not attracted to water, and ends up in the organic phase. Hence, the salt is located at the interface between the two phases. The aim of this master's thesis was to find out how the interfacial tension and the size of the two-phased region were influenced by addition of antagonistic salt.

The work was conducted by preparing seven mixtures composed of water and the organic solvent, with different concentrations of salt. The systems were constructed and simulated by means of molecular dynamics simulations.

The simulated results showed that the interfacial tension decreases as concentration of salt increases. Further, the results showed that the size of the two-phased region is reduced as the concentrations of salt increases, and that the region completely disappears for higher concentrations. The system then consists exclusively of a homogeneous phase.

Sammendrag

Blandinger av vann og organiske løsninger er veldig vanlig. De finnes i alt fra menneskekroppen til flere industriprosesser. Ved høyere og lavere temperaturer vil en blanding, som består av vann og den organiske løsningen 2,6-lutidin, forme en homogen fase. Mellom disse temperaturene vil det formes et tofase-område, bestående av en vannfase og en organisk fase. Denne masteroppgaven studerer variasjoner i spenning i tofase-området ved tilsetning av et antagonistisk salt.

Et antagonistisk salt er et salt som består av en hydrofil og en hydrofob del. Den hydrofile delen er tiltrukket av vannet, og vil løses i vannfasen. Den hydrofobe delen blir derimot frastøtt av vann, og vil ende opp i den organiske fasen. Saltet vil derfor befinne seg i grenseskillet mellom de to fasene. Målet med denne masteroppgaven er å finne ut hvordan grensespenningen påvirkes av tilsetningen av antagonistisk salt.

Dette ble gjort ved å konstruere syv blandinger bestående av vann og 2,6-lutidin med ulike konsentrasjoner av salt. Systemene ble konstruert og simulert ved hjelp av molekylærdynamikk.

Resultatene av simuleringene viser at grensespenningen synker ettersom konsentrasjonen av salt øker. I tillegg vises det at størrelsen på tofase-området minker når konsentrasjonen av salt øker, og området kan forsvinne helt ved høyere konsentrasjoner. Et slikt system består da utelukkende av en homogen fase.

Contents

Preface	i
Abstract	iii
Sammendrag	v
Contents	vii
List of Figures	xi
List of Tables	xv
1 Introduction	1
1.1 Background	1
1.2 Aim of Thesis	1
1.3 Detailed Objectives	2
1.4 Thesis Structure	2
2 Water/oil mixtures and antagonistic salts	5
2.1 Water	5
2.1.1 TIP4P/2005	6
2.2 2,6-lutidine	7
2.2.1 2,6-lutidine Model	7
2.3 Binary Mixture of Water and 2,6-Lutidine	9
2.4 Tension Between Two Phases	10
2.4.1 Surface Tension	10
2.4.2 Interfacial Tension	10
2.5 Antagonistic Salts	12
2.5.1 A General Overview	12
2.5.2 PPh ₄ Cl	13
2.5.3 PPh ₄ Cl Model	13
3 MD simulations	15
3.1 Classical Dynamics	15
3.1.1 Macroscopic Properties	15
3.1.2 Basic Principles of MD Simulations	16
3.2 Gromacs MD Package	17
3.3 MD Algorithms	17
3.3.1 Hydrogen Bonds	17
3.3.2 Partial Density Profiles	18
3.3.3 Radial Distribution Function	18

3.3.4	Energies	19
3.3.5	Interfacial Tension	20
4	MD simulations of the systems	21
4.1	Initial Composition of Water/2,6-Lutidine System	21
4.2	MD Simulations with Gromacs	23
4.3	Preparation	26
4.3.1	Water/2,6-Lutidine System	26
4.3.2	Water/2,6-Lutidine System with PPh ₄ Cl	27
4.4	MD Simulations	28
5	Results	31
5.1	Analysis	31
5.2	Molecular Configurations	33
5.3	Partial Density Profiles	37
5.4	Graphical Representation of Results	40
5.5	Simulation Results	44
6	Discussion	45
6.1	Simulation Parameters	45
6.1.1	Simulation Times	45
6.1.2	Temperature and Pressure Coupling	45
6.2	Molecular Configurations and Partial Density Profiles	46
6.2.1	Binary Mixture of Water and 2,6-Lutidine	46
6.2.2	Systems with Low Concentrations of PPh ₄ Cl	47
6.2.3	Systems with Medium Concentrations of PPh ₄ Cl	48
6.2.4	Systems with High Concentrations of PPh ₄ Cl	48
6.3	Hydrogen Bonds	49
6.4	Intermolecular Potential Energy	49
6.5	Molar Heat Capacity at Constant Pressure	50
6.6	Interfacial Tension	50
6.7	Sources of Error	50
7	Conclusion	51
8	Further Work	53
	References	54
	Appendices	61
	Appendix A Basics of Gromacs	61
A.1	Periodic Boundary Conditions	61
A.2	Molecular Interactions	62
A.2.1	Non-bonded Interactions	62
A.2.2	Bonded Interactions	63
A.3	Force Fields	64

A.4	Electrostatics	64
A.5	Statistical Ensembles	64
A.6	Coupling Algorithms	65
A.6.1	Temperature Coupling	65
A.6.2	Pressure Coupling	65
A.7	Constraint Algorithms	66
A.8	Central Gromacs Diles	66
Appendix B Gromacs Programs		68
Appendix C Gromacs Parameter Files		70
C.1	TIP4P/2005 and 2,6-Lutidine	70
C.1.1	Energy Minimization	70
C.1.2	Equilibration Run	71
C.1.3	Production Run	72
C.2	Water/2,6-Lutidine Mixture with Salt	73
C.2.1	Energy Minimization	73
C.2.2	Equilibration Run	74
C.2.3	Production Run	75

List of Figures

2.1	Structural formula (a) and 3D model of the van der Waals spheres (b) of H ₂ O. Red indicate oxygen and white hydrogen atoms.	6
2.2	A TIP4P/2005 water model molecule. Red indicate the oxygen atom, white hydrogen atoms, and yellow indicate the M site. δ^+ and δ^{2-} indicates the partial positive and negative charges for the model [63].	6
2.3	Structural formula (a) and 3D model (b) of C ₇ H ₉ N. Blue indicate nitrogen, grey carbon, and white hydrogen atoms.	8
2.4	2,6-lutidine molecule with final partial charges [47]. CH ₃ -groups are treated as single atoms. The total charge of the molecule is zero.	8
2.5	Illustration of bulk phase diagram of water/2,6-lutidine system at constant volume, based on the work completed by Gambassi et al.. <i>C</i> _{2,6-lutidine} denotes mass fraction. UCP and LCP indicates upper and lower critical points, describing the outline of the coexistence loop, with associated temperatures T_{UCP} and T_{LCP} . Insets (i) and (ii) shows the schematic side views of vertical cells of the two-phase and homogeneous phase. Inset (i) shows the oil-rich phase (L) and the water-rich phase (W) [14].	9
2.6	Simplified illustration of interfacial tension in two different systems. Figure (a) illustrates surface tension between water and air, and (b) illustrates interfacial tension between water and organic liquid. The blue solid arrows in (a) indicates cohesive forces, and the transparent arrows indicates missing cohesive forces due to fewer neighbouring molecules. The blue and red solid arrows in (b) indicates cohesive forces, and the dotted arrows indicates adhesive forces.	11
2.7	Schematic illustration of the distribution of an antagonistic salt along the interface of a water/organic solvent system. Hydrophilic and hydrophobic ion pairs are distributed along the interface. Hydrophilic ions will dissolve in the water-rich region and hydrophobic ions in the 2,6-lutidine-rich region.	12
2.8	Structural formula (a) and 3D model (b) of PPh ₄ Cl. Green indicate chlorine, orange phosphorus, grey carbon, and white hydrogen atoms.	14
2.9	Schematic illustration of the distribution of PPh ₄ Cl along the interface of a water/2,6-lutidine system. Hydrophilic anions (Cl ⁻) will dissolve in the water-rich region and hydrophobic cations (PPh ₄ ⁺) in the 2,6-lutidine-rich region.	14
3.1	Geometric criterion for verification of the existence of a hydrogen bond.	18

3.2	A list of the different quantities that can be chosen from the Gromacs program <i>gmx energy</i> . The abbreviation LUT refers to 2,6-lutidine, SOL to TIP4P/2005, CL to chloride anions, and _WEO to PPh ₄ ⁺ . See the Gromacs reference manual for details of all energy terms [35].	19
4.1	Illustration of the bulk phase diagram of water/2,6-lutidine system at constant volume. C _{2,6-lutidine} denotes mass fraction of 2,6-lutidine. UCP and LCP indicates the upper and the lower critical point, describing the outline of the coexistence loop [14]. The green - - line indicates mass fraction of 2,6-lutidine of the initial system, and the green ·· line indicates the simulation temperature $T_{sim} = 380$ K for all systems. Point <i>P</i> indicates where the the two lines intercept, and where the initial system is located.	22
4.2	Outline of a MD simulation by Gromacs [33]. Each step is connected to a dotted box that describes which Gromacs programs run, which files created, and additional programs that are run to fulfill each step.	24
5.1	Quantities during production run for the water/2,6-lutidine system with 0.00 mol% PPh ₄ Cl. Graph (a) is of temperature, (b) density, (c) potential energy per molecule, (d) volume, (e) Coulomb short range electrostatic interactions, and (f) short range intramolecular LJ interactions.	32
5.2	Molecular configuration of the water/2,6-lutidine system with 0.00 mol% PPh ₄ Cl after 286 ns of NPT simulation. Blue points indicate water and orange 2,6-lutidine.	33
5.3	Molecular configuration of the water/2,6-lutidine system with 0.05 mol% PPh ₄ Cl after 266 ns of NPT simulation. Blue points indicate water and orange 2,6-lutidine. Green spheres illustrates Cl ⁻ anions and orange spheres PPh ₄ ⁺ cations.	34
5.4	Molecular configuration of the water/2,6-lutidine system with 0.14 mol% PPh ₄ Cl after 254 ns of NPT simulation. Blue points indicate water and orange 2,6-lutidine. Green spheres illustrates Cl ⁻ anions and orange spheres PPh ₄ ⁺ cations.	34
5.5	Molecular configuration of the water/2,6-lutidine system with 0.27 mol% PPh ₄ Cl after 254 ns of NPT simulation. Blue points indicate water and orange 2,6-lutidine. Green spheres illustrates Cl ⁻ anions and orange spheres PPh ₄ ⁺ cations.	35
5.6	Molecular configuration of the water/2,6-lutidine system with 0.36 mol% PPh ₄ Cl after 257 ns of NPT simulation. Blue points indicate water and orange 2,6-lutidine. Green spheres illustrates Cl ⁻ anions and orange spheres PPh ₄ ⁺ cations.	35
5.7	Molecular configuration of the water/2,6-lutidine system with 0.45 mol% PPh ₄ Cl after 300 ns of NPT simulation. Blue points indicate water and orange 2,6-lutidine. Green spheres illustrates Cl ⁻ anions and orange spheres PPh ₄ ⁺ cations.	36
5.8	Molecular configuration of the water/2,6-lutidine system with 1.36 mol% PPh ₄ Cl after 2760 ns of NPT simulation. Blue points indicate water and orange 2,6-lutidine. Green spheres illustrates Cl ⁻ anions and orange spheres PPh ₄ ⁺ cations.	36
5.9	Density profile of the water/2,6-lutidine system with (a) 0.00 mol%, (b) 0.14 mol%, (c) 0.36 mol%, and (d) 1.36 mol% PPh ₄ Cl averaged over time from 150 ns to 286 ns, 254 ns, 257 ns, and 276 ns respectively.	37
5.10	Density profile of water and lutidine in the water/2,6-lutidine system with (a) 0.00 mol%, (b) 0.14 mol%, (c) 0.36 mol%, and (d) 1.36 mol% PPh ₄ Cl averaged over time from 150 ns to 286 ns, 254 ns, 257 ns, and 276 ns respectively.	38

5.11	Density profile of hydrophobic cations PPh_4^+ and hydrophilic anions Cl^- in the water/2,6-lutidine system with (a) 0.14 mol%, (b) 0.36 mol%, and (c) 1.36 mol% PPh_4Cl averaged over time from 150 ns to 286 ns, 254 ns, 257 ns, and 276 ns respectively.	39
5.12	Total density $\rho(t)$ of the water/2,6-lutidine system with different mol% of PPh_4Cl , from 25 ns of simulation with NPT at $T_{sim} = 380$ K and $p_{sim} = 1$ bar.	40
5.13	Number of hydrogen bonds between water and 2,6-lutidine per 2,6-lutidine molecule for all systems with different mol% of PPh_4Cl at $T_{sim} = 380$ K and $p_{sim} = 1$ bar.	41
5.14	Potential energy $U(t)$ between all molecules in the system per molecule of water for all systems with different mol% of PPh_4Cl at $T_{sim} = 380$ K and $p_{sim} = 1$ bar.	42
5.15	Interfacial tension $\gamma(t)$ for all systems with different mol% of PPh_4Cl at $T_{sim} = 380$ K and $p_{sim} = 1$ bar.	43
6.1	Illustration of the innermost hydration shell surrounding a chloride anion. The green atom in the middle is the chloride anion, with water molecules around. δ^+ and δ^{2-} indicates the partial charges of the water molecules.	47
A.1	Periodic boundary conditions: The original system (dark particles) surrounded by replicas [3].	62
A.2	The Lennard Jones interaction [35].	63

List of Tables

4.1	Overview of the seven systems simulated, composed of the antagonistic salt PPh ₄ Cl, water, and the organic solvent 2,6-lutidine (C ₇ H ₉ N). The concentrations of the components are expressed by the number of molecules and by mol%.	28
4.2	Overview of the time lengths for the simulations for all seven systems. NVT indicates the length of simulation by canonical ensemble, and NPT by isothermal-isobaric ensemble.	29
5.1	Simulated results for for various physical quantities of the water/2,6-lutidine system with different salt concentrations after NPT at $T_{sim} = 380$ K. The symbol ρ denotes density of the whole system, T temperature, p pressure, C_p heat capacity at constant pressure, U potential energy, and γ interfacial tension. C_p and U are calculated per molecule of the system. and γ is given for the entire bilayer. All quantities were simulated with the Parrinello-Rahman barostat, except γ which was simulated with Berendsen.	44
5.2	Average number of hydrogen bonds between water and water per water molecule, and between water and 2,6-lutidine per 2,6-lutidine molecule.	44
B.1	Gromacs programs used in MD simulations.	69

Chapter 1

Introduction

1.1 Background

Binary mixtures consisting of water and organic solvents are very common. They are found inside our bodies and in many industrial settings. Most organic solvents separates from water and the binary mixture will usually be composed of two separate phases with an interface between them. It is well established that addition of different types of salt may change the properties of binary mixtures, one of which is interfacial tension [42, 51, 53, 59]. Lyklema [31] describes interfacial tension as the tension on the surfaces of two immiscible liquids, where the tension takes place due to unbalanced intermolecular forces. Knowledge about interfacial tension plays an important role in many applications and industries, such as oil recovery, drug delivery, biochemical research, and coating and dispersion processes [34].

If antagonistic salts are added to binary mixtures described above, the properties of the mixtures can change significantly [54]. Antagonistic salts consists of hydrophilic and hydrophobic ions. If added to a water/organic solvent mixture, hydrophilic ions will dissolve in the water phase and hydrophobic ions in the organic phase [49, 54, 65]. The salts will position at the interfaces in the mixture [50]. Among the consequences of introducing antagonistic salt is reduction of the interfacial tension [44, 53]. Experiments done by Luo et al. shows that by increasing the concentration of antagonistic salts the interfacial tension can be reduced even further [30].

1.2 Aim of Thesis

This master's thesis will study the effect antagonistic salts has on the interfacial tension in a binary mixture consisting of water and organic solvent at constant pressure and temperature. This will be studied by adding different concentrations of antagonistic salt to a binary mixture. The binary mixture consists of water/2,6-lutidine and the antagonistic salt tetraphenylphosphonium chloride (PPh_4Cl).

The hypothesis that the interfacial tension in this kind of system, will decrease with increasing concentrations of salt. The aim of this thesis is to confirm the reduction of interfacial tension. The study will be completed by means of molecular dynamics (MD) simulations, using the MD package Gromacs.

1.3 Detailed Objectives

To study the effect of different salt concentrations on the interfacial tension, seven systems with increasing concentrations will be simulated at constant pressure and temperature, respectively $p_{sim} = 1$ bar and $T_{sim} = 380$ K. The systems consists of water, the organic solvent 2,6-lutidine (C_7H_9N), and the antagonistic salt tetraphenylphosphonium chloride (PPh_4Cl). 2,6-lutidine is a natural organic compound miscible in water [37], whereas PPh_4Cl is an antagonistic salt which consists of one hydrophobic part (PPh_4^+) and one hydrophilic part (Cl^-).

Each system contain the same amount of 2,6-lutidine and different amounts of water and salt. The concentration of salt will range from 0 mol% to 1.36 mol% with respectively 86.36 mol% to 85.00 mol% water. All systems consist of 13.64 mol% 2,6-lutidine. Table 4.1 shows the mole percent for all seven systems. Even though the concentration of salt is fairly small compared to the rest of the system, it is expected that the additions will influence the properties of the systems.

To simulate the systems a model of each component is required. Water is simulated by the TIP4P/2005 water model proposed by Abascal and Vega, as it is the currently best model of condensed phases of water [63]. The 2,6-lutidine model proposed by Pousaneh et al. is selected as it successfully describes, the bulk 2,6-lutidine liquid and water/2,6-lutidine properties [47]. The model used to describe tetraphenylphosphonium (PPh_4^+) were parameterized by the co-supervisor of this thesis, Faezeh Pousaneh. This model, in combination with chloride anions, results in PPh_4Cl .

The simulations are computed by the supercomputer Vilje to reduce the time consumed to simulate the systems [19]. Vilje is a cluster system produced by NTNU in collaboration with met.no and UNINETT Sigma [60]. MD simulations are done by the MD package Gromacs. Gromacs is a user-friendly free full-featured molecular dynamics simulation package which is well-suited for parallelization on processor clusters [2, 61].

1.4 Thesis Structure

This master's thesis contains seven chapters and three appendices. The second chapter is called *2 Water/oil mixtures and antagonistic salts*, and the third *3 MD simulations*, which presents relevant theory for this thesis. This includes description of binary systems consisting of water and an organic solvent, interfacial tension and a study of antagonistic salts. In addition will the organic solvent 2,6-lutidine and the antagonistic salt PPh_4Cl be described in detail, as well as the models used in MD simulations. The third chapter describes the basics for MD simulation in short and a general introduction to the MD simulation package Gromacs is given.

In the next chapter, *4 MD simulations of the systems*, the method used to conduct MD simulations is described. Additionally, a discussion of the initial composition is included, as well as descriptions of Gromacs algorithms used. The way the systems were analyzed and the results are presented in chapter *5 Results*, by molecular configurations, values, and graphs.

The last part of the thesis contains chapter *6 Discussion* and *7 Conclusion*. The results of the MD simulations are discussed in the context of the already reviewed theory, followed by concluding remarks on the work and results.

Three appendices are enclosed; *A Basics of Gromacs*, *B Gromacs Programs*, and *C Gromacs Parameter Files*. The appendices are not essential for a general understanding of the completed work, but can be seen as an addition. Appendices A and B and works as small encyclopedias for Gromacs. Appendix C contains all parameter files used in this thesis MD simulation.

Chapter 2

Water/oil mixtures and antagonistic salts

2.1 Water

The properties of water (H_2O) can be described through its molecular structure, shown in figure 2.1. The bent structure of the molecule is the result of the repulsive effect of the two sets of lonely electrons, the two lone pairs [18, 48]. The H–O–H angle is 105.5° . The length of the O–H bonds are 0.991 \AA [58]. The molar mass of water is approximately 18.0153 grams per mole [38]. Water molecules have polar composition, where oxygen has partial negative charge and hydrogen partial positive charge. The shared electrons in the O–H bonds will be more attracted to the oxygen atom, because of higher electronegativity. The bonds inside a water molecule is classified as polar covalent bonds. Because of the polar covalent bonds and the bent shape, water is classified as a polar molecule [5].

In water, hydrogen bonds are found between hydrogen atoms in one molecule and oxygen atoms in another. Hydrogen bonds are dipole-dipole bonds that forms when a hydrogen atom is in close proximity of a higher electronegativity atom, like oxygen [45].

As a result of the polarity, electrostatic interactions forms between water and ions or other polar molecules. If the ratio between water and solute is high enough, hydration shells forms around the solute and evenly distributes it throughout the water. When the system reaches equilibrium, the solute will disperse in water. Ions and polar molecules with these properties is said to be hydrophilic [48]. Nonpolar molecules do not interact with water in the same way, as they do not form electrostatic interactions with water. The result is formation of droplets or layers consisting of nonpolar molecules. Nonpolar molecules with these properties is said to be hydrophobic [5].

2.1.1 TIP4P/2005

The TIP4P/2005 water model, shown in figure 2.2, has been developed as a general model for the condensed phases of water [9]. TIP4P/2005 is a rigid four site non-polarized water model, where the intergranular degrees of freedom are frozen. The angle between O-H bonds is set to 104.53° , and the H-O distance is fixed and set to 0.9572 \AA [1, 15, 63]. The model is planar, has one Lennard-Jones center, and three fixed point charges. The oxygen site contributes to the Lennard-Jones term, but has no charge. The positive partial electrostatic charges are placed at the hydrogen atoms, the hydrogen sites (δ^+). The partial negative charge is placed at the M site (δ^{2-}). Note that the total charge is zero. The M site represents a non-physical mass-less but charged site placed at the bisector of the H-O-H angle. The hydrogen sites and the M site does not contribute to the Lennard-Jones term [1]. In 2011 Vega and Abascal tested rigid non-polarized water models for different properties and concluded that TIP4P/2005 is a reasonable accurate water model [63].



Figure 2.1: Structural formula (a) and 3D model of the van der Waals spheres (b) of H₂O. Red indicate oxygen and white hydrogen atoms.

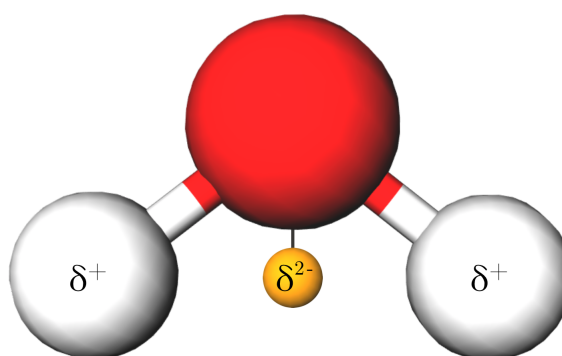


Figure 2.2: A TIP4P/2005 water model molecule. Red indicate the oxygen atom, white hydrogen atoms, and yellow indicate the M site. δ^+ and δ^{2-} indicates the partial positive and negative charges for the model [63].

2.2 2,6-lutidine

2,6-lutidine (C_7H_9N) can be characterized as a natural heterocyclic aromatic organic compound with moderate basic properties. The compound is one of many pyridine derivatives, and is also known as 2,6-dimethylpyridine. The molar mass of 2,6-lutidine is 107.156 grams per mole [37]. 2,6-lutidine represents the organic solvent in the binary system described in section 2.3, and can be described as an oil. It is miscible in water as it can form hydrogen bonds with water at lower and higher temperatures, as seen in figure 2.5. In the miscibility gap, the two fluids are immiscible [47, 56].

Figure 2.3 illustrate 2,6-lutidine through the structural formula and a 3D model. The 2,6-lutidine molecule is formed as a hexagon composed by five carbon atoms and one nitrogen atom. Two of the five carbon atoms in the ring have a methyl group (CH_3) attached, where the rest has a hydrogen atom. These basic properties are results of the lone pairs at the nitrogen atom [56].

2.2.1 2,6-lutidine Model

The liquid model used in this thesis consists of 11 atoms: five carbon atoms, three hydrogen atoms, one nitrogen atom, and two CH_3 groups. This is six atoms less than the 2,6-lutidine molecule has in reality, caused by treating the CH_3 groups as united atoms in the model.

The partial charges of the atoms are stated next to the associated atom in figure 2.4. The partial charges on 2,6-lutidine are not provided by the GROMOS force field, which is used in MD simulations with Gromacs, so the charges were configured by Pousaneh et al. to reflect bulk properties of 2,6-lutidine liquid [47]. The total charge of the molecule is zero. See appendix A.3 for more details about force fields.

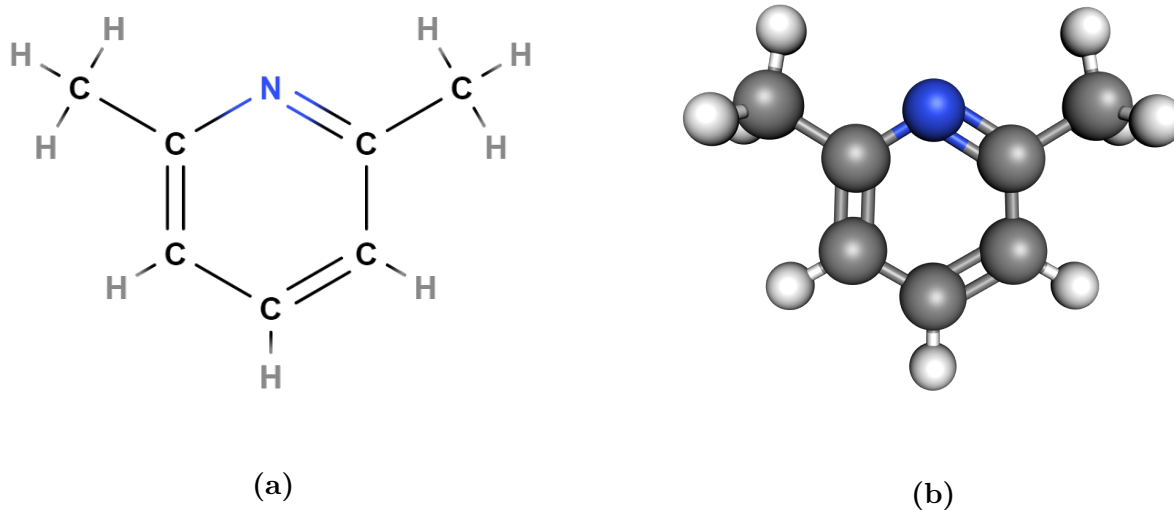


Figure 2.3: Structural formula (a) and 3D model (b) of C₇H₉N. Blue indicate nitrogen, grey carbon, and white hydrogen atoms.

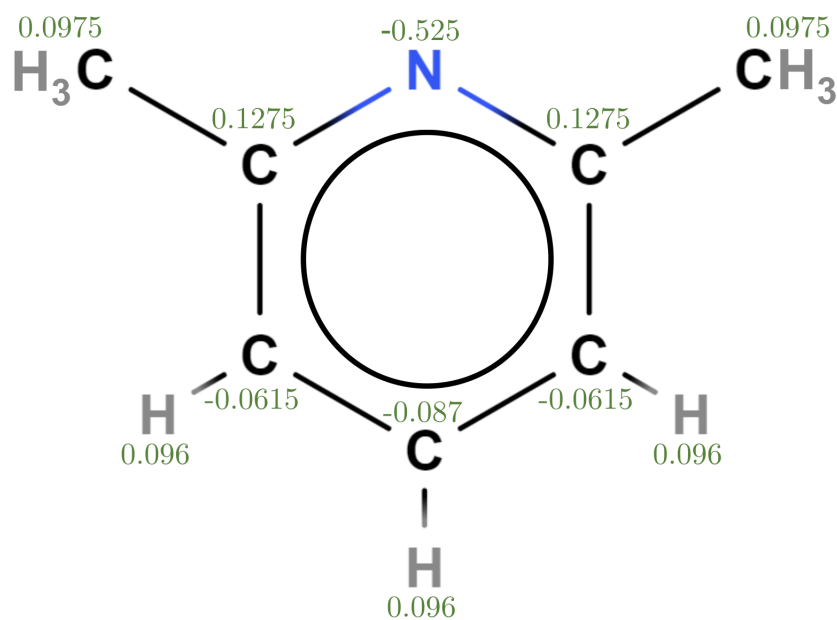


Figure 2.4: 2,6-lutidine molecule with final partial charges [47]. CH₃-groups are treated as single atoms. The total charge of the molecule is zero.

2.3 Binary Mixture of Water and 2,6-Lutidine

Phase diagrams of liquid binary mixtures consisting of water and organic solvent, can be a so called closed-loop phase diagram with a miscibility gap [14]. Inside a miscibility gap, also known as a coexistence loop, the mixture will disintegrate and separate into two phases. This is also valid for a mixture of water/2,6-lutidine, shown in figure 2.5. The diagram consists of both a lower (LCP) and upper critical point (UCP). Outside the coexistence loop, one homogeneous mixed phase will be present. This is typically at temperatures below LCP, $T < T_{LCP} = 307.15\text{K}$, and above UCP, $T > T_{UCP} (> 500 \text{ K})$ [14, 36].

The mechanisms behind the appearance of UCP and LCP, are outlined by Pousaneh et al. The way the two phases mix and separate could be caused by formation of directional bonds, such as hydrogen bonds, between water and 2,6-lutidine. In the region below LCP, hydrogen bonding between water and 2,6-lutidine will boost formation of a homogeneous phase. The hydrogen bonds that promoted the homogeneous phase will be destroyed in the miscibility gap. The destruction is due to thermal fluctuations [47]. The schematic side view of the miscibility gap is shown by inset (i) in figure 2.5. The two-phase coexistence loop, consists of a 2,6-lutidine-rich phase (L) and a water-rich phase (W) illustrated by the inset. Inset (ii) shows the side view of the homogeneous phase outside the miscibility gap [14].

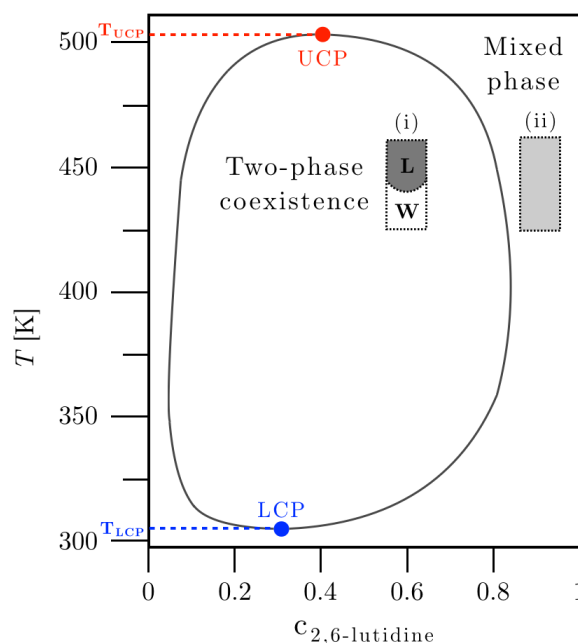


Figure 2.5: Illustration of bulk phase diagram of water/2,6-lutidine system at constant volume, based on the work completed by Gambassi et al.. $C_{2,6-lutidine}$ denotes mass fraction. UCP and LCP indicates upper and lower critical points, describing the outline of the coexistence loop, with associated temperatures T_{UCP} and T_{LCP} . Insets (i) and (ii) shows the schematic side views of vertical cells of the two-phase and homogeneous phase. Inset (i) shows the oil-rich phase (L) and the water-rich phase (W) [14].

2.4 Tension Between Two Phases

Interfacial tension is a general term describing tension that occurs between two phases in a system, as shown in figure 2.6. Tension between a gas and a liquid (surface tension, figure 2.6a) and between two immiscible liquids (interfacial tension, figure 2.6b) will both be discussed in the two following sections [12].

2.4.1 Surface Tension

In a system consisting of liquid and gas, e.g. water and air, a surface occurs between the two phases as shown in figure 2.6a. Molecules in the bulk are completely surrounded by neighbouring molecules, whereas molecules close to the surface are not. All neighbouring molecules in a substance attract each other with equal force. These intermolecular forces, e.g. Van der Waals forces, are called cohesive forces [8], and are illustrated by solid arrows in figure 2.6. Surface molecules are only influenced by cohesive forces on one side, as shown in figure 2.6a. Molecules close to the surface have different binding energies than the molecules in the bulk [27]. Cohesive forces will pull surface molecules in towards the bulk, making the liquid shrink into the form with minimum surface area. This uneven distribution of cohesion forces generates tension on the liquid surface, called surface tension [29, 46].

2.4.2 Interfacial Tension

Lyklema [31] explains interfacial tension in two ways, thermodynamically and mechanically. Thermodynamically interfacial tension can be described as if an area of an interface is increased reversibly by an amount dA at constant temperature and composition, and in addition constant volume or pressure, the Helmholtz or Gibbs energy of the system will increase. This change is described as the interfacial tension, and can be expressed by equation 2.1 by respectively Helmholtz (F) and Gibbs energy of the system (G),

$$\gamma = \left(\frac{\partial F}{\partial A} \right)_{V,T,n} \qquad \gamma = \left(\frac{\partial G}{\partial A} \right)_{p,T,n} \qquad (2.1)$$

where V , T , and p is constant volume, temperature and pressure, respectively. n denotes different amounts n_1, n_2, \dots, n_n which describes the composition of the system.

Mechanically interfacial tension can be described as the contractive force per unit length acting on the interface and its parallels. The dimension of interfacial tension γ is force divided by length with unit N m^{-1} .

When the system is at equilibrium the results of the means are equal, and can be called static interfacial tensions. Under non-equilibrium conditions there will be dynamic interfacial tension, and the only valid way to calculate it is mechanical. If a surface is established rapidly, then relaxes relatively slow over a time frame τ , the surface is still at a non-equilibrium state after a time t , where $t < \tau$. This way the time dependent interfacial tension $\gamma(t)$ is found [26, 31].

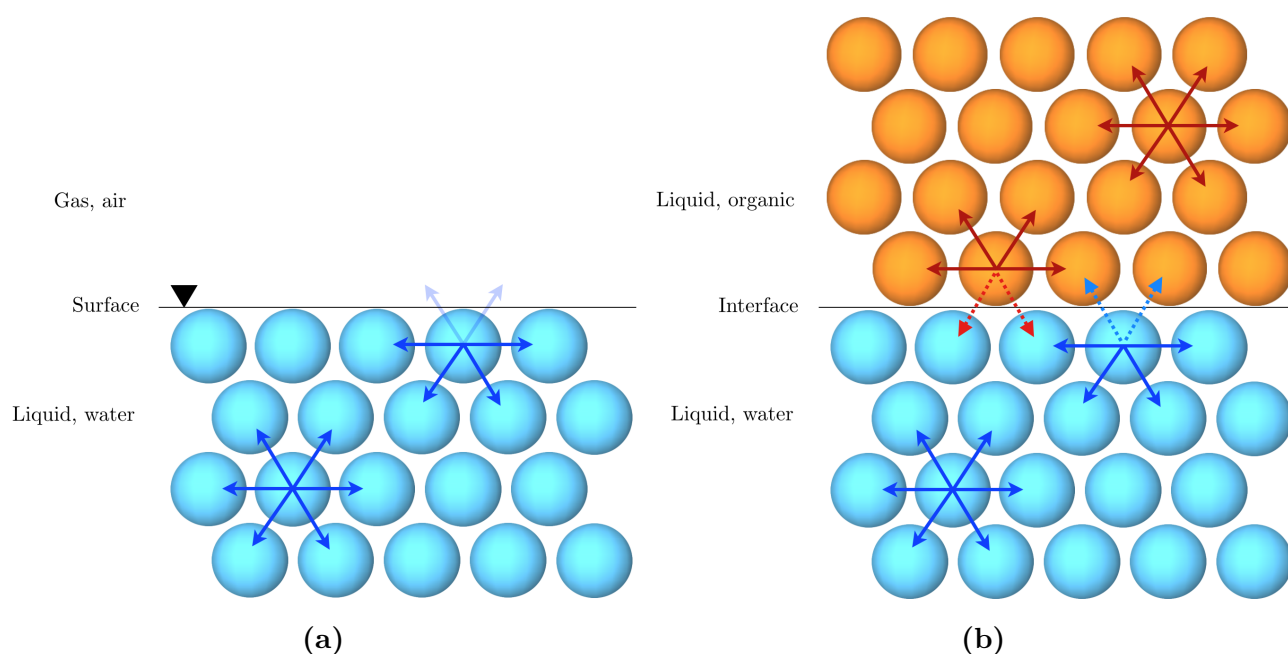


Figure 2.6: Simplified illustration of interfacial tension in two different systems. Figure (a) illustrates surface tension between water and air, and (b) illustrates interfacial tension between water and organic liquid. The blue solid arrows in (a) indicates cohesive forces, and the transparent arrows indicates missing cohesive forces due to fewer neighbouring molecules. The blue and red solid arrows in (b) indicates cohesive forces, and the dotted arrows indicates adhesive forces.

2.5 Antagonistic Salts

2.5.1 A General Overview

It is well established that "normally antagonistic" salts composed of hydrophilic inorganic cations and hydrophobic organic anions [32, 34, 41, 44, 49, 53, 57, 66]. In a binary mixture consisting of water and the organic solvent 2,6-lutidine, hydrophilic ions dissolve in the water phase and hydrophobic ions in the organic solvent phase. The salt then forms ion pairs across the interface [65]. Figure 2.7 schematically illustrates the interface of the system with antagonistic salt, and how the different parts of the salt dissolves in the system.

A "normally antagonistic" salt is composed by a hydrophilic cation and a hydrophobic anion, as sodium tetraphenylborate (NaBPh_4), with the hydrophilic cation Na^+ and the hydrophobic anion BPh_4^- . An "inversely antagonistic" salt is composed of a hydrophilic anion and a hydrophobic cation. An example is the salt used in this thesis; tetraphenylphosphonium chloride (PPh_4Cl), which is composed of a hydrophilic anion Cl^- and a hydrophobic cation PPh_4^+ [32, 52]. There are differences between the two types of antagonistic salt, but Sadakane and Seto indicate that the "inversely antagonistic" salt PPh_4Cl will increase the mutual solubility in a water/organic solvent mixture, as a "normally antagonistic" salt will do [49, 52]. As this thesis studies the interfacial tension, an "inversely antagonistic" salt can and will, be used to study the effect of an antagonistic salt in a water/2,6-lutidine mixture.

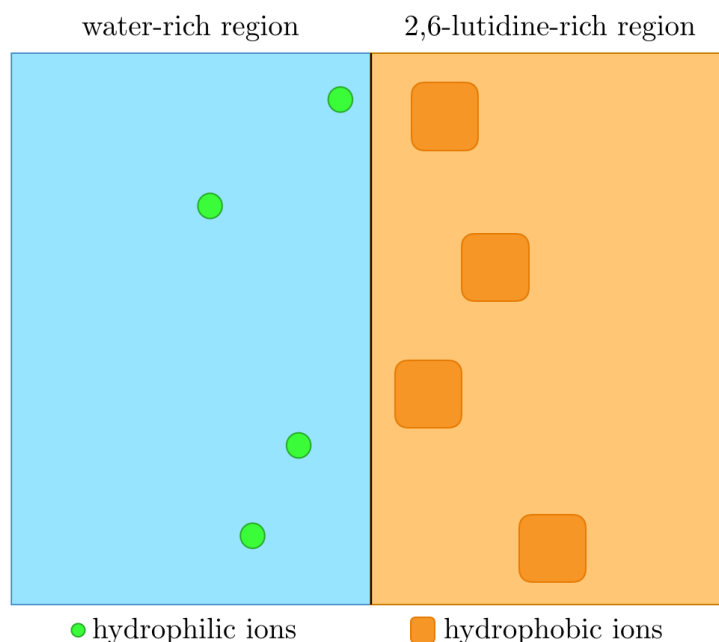


Figure 2.7: Schematic illustration of the distribution of an antagonistic salt along the interface of a water/organic solvent system. Hydrophilic and hydrophobic ion pairs are distributed along the interface. Hydrophilic ions will dissolve in the water-rich region and hydrophobic ions in the 2,6-lutidine-rich region.

Experiments shows that small concentrations of antagonistic salts can change the properties of a water and organic solvent mixture significantly [54]. The salt will undergo microphase separation at the interface of a Debye screening length. The hydrophilic anions (Cl^-) and hydrophobic cations (PPh_4^+) tends to spontaneously adsorb close to the interface [34, 43, 49]. The ion distribution produces an electric double layer at the interface. Water molecules surrounding inorganic anions will form hydration shells and the anions will be strongly hydrophilic. Hydrogen bonds surrounding larger organic cations will be deformed and the cations will acquire hydrophobicity [44, 49]. Experiments done by Luo et al. [30] shows that by increasing the concentration of antagonistic salt the interfacial tension will be reduced, as well as the miscibility gap. The interfacial tension can even become negative at high enough concentrations [23, 43]. At high concentrations the miscibility gap, described in section 2.3, can even disappear completely [49, 53].

2.5.2 PPh_4Cl

Tetraphenylphosphonium chloride PPh_4Cl is classified as an antagonistic salt, composed of hydrophilic anions (Cl^-) and hydrophobic cations (PPh_4^+) [52, 54, 65]. The structural formula for the salt is shown in figure 2.8a. "Ph₄" in PPh_4Cl represent four phenyl rings ($(\text{C}_6\text{H}_5)_4$) bonded to the phosphorus atom [49]. A 3D model of the structure is shown in figure 2.8b. The molar mass of PPh_4Cl is 374.848 grams per mole [39].

As described in section 2.5.1, PPh_4Cl tends to adsorb around the interfaces of a water/2,6-lutidine mix due to selective solvation. The hydrophilic effect of Cl^- anions comes from surrounding water molecules which creates hydration shells around the ions in water. PPh_4^+ is strongly hydrophobic because of the four largely sized phenyl rings which leads to deformation of the surrounding hydrogen bonding, and in the end destruction of the surrounding hydration shells. In other words, Cl^- ions dissolves in the water-rich region and PPh_4^+ dissolves in the 2,6-lutidine-rich region as shown in figure 2.9 [44, 49]. Sadakane et al. confirms that the miscibility gap described in section 2.3 does shrink with addition of PPh_4Cl [52].

2.5.3 PPh_4Cl Model

The salt model used to describe PPh_4Cl is composed of carbon and phosphorus atoms, and CH groups treated as single atoms. This thesis co-supervisor, Faezeh Pousaneh, parameterized the model. The model does not contain the chloride atom in PPh_4Cl , and describes only the phosphorus atom with the four phenyl rings, or in other words the hydrophobic cation PPh_4^+ . The model describes only one molecule of the cation, and the total charge of the molecule is +. To simulate the whole antagonistic salt, addition of a chloride anion Cl^- with a partial charge -1, is necessary. The salt model in combination with chloride anions will describe the antagonistic salt PPh_4Cl in MD simulations. The total charge of the model and the anion becomes zero.

The amount of chloride is equivalent to the number of molecules of PPh_4^+ . E.g. 10 models is equivalent to an addition of 10 chloride atoms. The chloride atoms are parameterized by the default partial charges for the GROMOS force field [35].

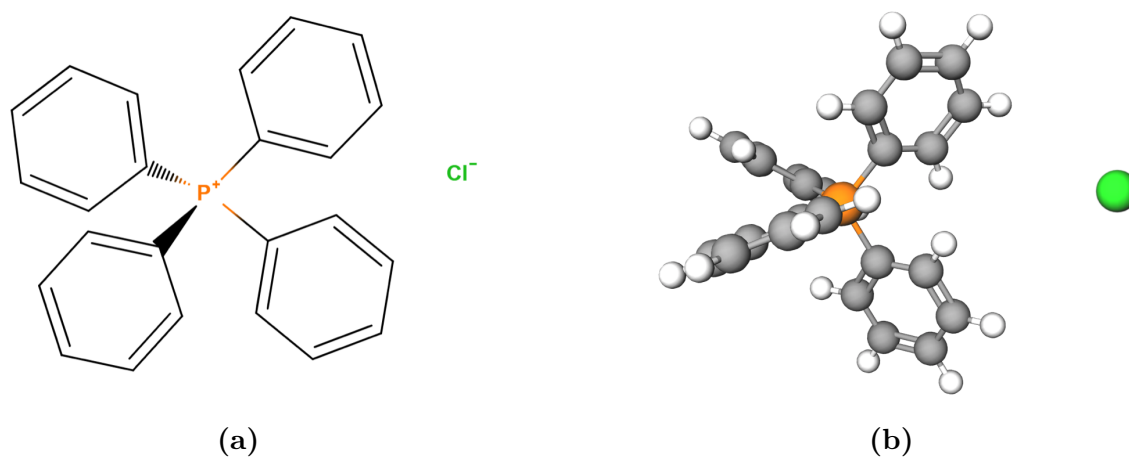


Figure 2.8: Structural formula (a) and 3D model (b) of PPh_4Cl . Green indicate chlorine, orange phosphorus, grey carbon, and white hydrogen atoms.

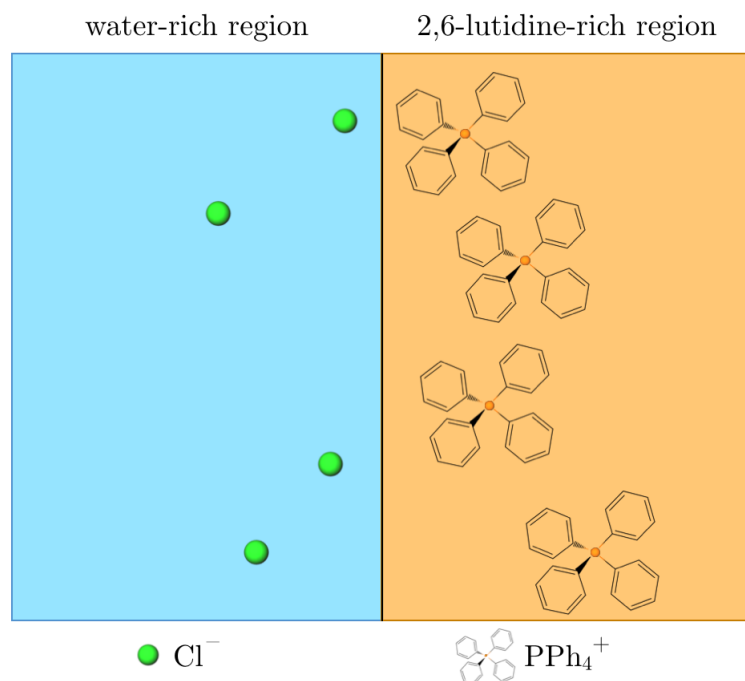


Figure 2.9: Schematic illustration of the distribution of PPh_4Cl along the interface of a water/2,6-lutidine system. Hydrophilic anions (Cl^-) will dissolve in the water-rich region and hydrophobic cations (PPh_4^+) in the 2,6-lutidine-rich region.

Chapter 3

MD simulations

This chapter is mainly based on the Gromacs reference manual written by M.J. Abraham and the rest of the Gromacs development team. For further reading and more details about Gromacs see appendix A, B, and C, or the Gromacs user manual [35].

3.1 Classical Dynamics

Molecular dynamics (MD) can be seen as a complement to traditional and conventional experiments. With MD the properties of different molecules can be understood when it comes to their structure and interactions between them [3]. With MD it is possible to describe complex chemical systems that are built atom by atom. The aim of MD is ultimately to predict and understand properties on a macroscopic scale, based on microscopic interactions [62].

The results of MD simulations are trajectories for a system, based on coordinates as a function of time. After a simulation time t , the system will approach an equilibrium state. As it is difficult to simulate the perfect equilibrium state of a system, the systems are simulated over a long time period so they can be said to be at equilibrium. Different macroscopic properties can be found based on these systems.

3.1.1 Macroscopic Properties

Macroscopic properties are categorized as static equilibrium or dynamic non-equilibrium properties. With the time-dependent Schrödinger equation, simulations of simple systems can be computed accurately. The time-dependent Schrödinger equation describes the state functions of quantum-mechanical systems, and describes how systems evolves with time [16]. For more complex chemical systems, e.g. systems consisting of few atoms in non-equilibrium state, the systems will not be simulated with the same accuracy. Approximations are then necessary, especially for more complex systems with long simulation times. At a point the ab initio way will be insufficient and it will be necessary to switch approaches to an empirical parameterization for

the model. For even more complex systems the simulations that are based on physical principles fail. The base for MD is then to analyze the structures and chemical data already known.

Macroscopic properties for different molecular systems are consequently averages. The use of these averages is important for MD in two ways. MD needs a representative set of data for a single structure at a fixed temperature. In addition extensions of MD simulation techniques are also needed for the computation of free energies and thermodynamic potentials. Second, the output of MD often contains irrelevant data about structures and motions that has next to nothing to do with the actual macroscopic properties studied. With this in mind, irrelevant data can be neglected.

To produce the required and representative set of data, there are two methods, or families, of simulation techniques; Molecular dynamics (MD) and Monte Carlo (MC). There are also many hybrids of these two techniques [3]. With MD it is possible to retain the actual trajectory of the system, which is not possible with traditional MC simulations. MC is a way to simulate computational algorithms which depends on repeated randomized sampling to obtain numerical data [40]. This master's thesis will, as mentioned in the introduction, use MD to simulate different systems.

3.1.2 Basic Principles of MD Simulations

MD is based on an evaluation of Newton's equations of motion. For an atom n ($n = 1, 2, \dots, N$) in a system, the force F_n that makes the atoms move in space, is given by equation 3.1

$$F_n = m_n \cdot \frac{\partial^2}{\partial t^2} r_n \quad (3.1)$$

where m_n is atomic mass and r_n atoms positions. The forces can be written as the negative derivatives of a potential energy function $V(r_1, r_2, \dots, r_N)$, as shown by equation 3.2

$$F_n = -\frac{\partial}{\partial r_n} V \quad (3.2)$$

which gives the relationship stated in equation 3.3

$$-\frac{\partial}{\partial r_n} V = m_n \cdot \frac{\partial^2}{\partial t^2} r_n \quad (3.3)$$

Molecular structures are introduced to the equations by the potential [3]. The equations are solved numerically with short time steps for every atom n . The size of the time step Δt is needed to be the largest time step possible, while there still is a stable motion of the molecules. A larger time step is preferred to reduce computing time [22].

3.2 Gromacs MD Package

Gromacs (Groningen Machine for Chemical Simulations) is a user-friendly free full-featured molecular dynamics simulation package. Gromacs is available under the GNU Lesser General Public License (LGPL). Gromacs is under constant development from their development teams at the Royal Institute of Technology and Uppsala University, Sweden [33].

With Gromacs the user can perform MD simulations, and produce trajectories of systems. Gromacs is well-suited for parallelization on processor clusters and runs well with the supercomputer used in this thesis, Vilje [2].

Gromacs can simulate both small and large systems with the use of usual and state-of-the-art algorithms. The program was originally designed to study proteins, lipids and nucleic acids, but is today also used to for studying a wide variety of other chemical and biological compounds [2, 33, 35].

Appendix A outlines some of the essential terms and basics of MD simulations with Gromacs. The appendix studies the periodic boundary conditions, molecular interactions (bonded and non-bonded), force fields, electrostatics, statistical ensembles, coupling algorithms (temperature and pressure coupling), and constraint algorithms. In addition the appendix gives a short review of the necessary Gromacs files. Appendix B describes Gromacs programs used in this thesis.

3.3 MD Algorithms

Gromacs uses a wide range of algorithms to calculate properties and quantities. This section describes the algorithms and methods used to obtain results from the MD simulations. The simulated systems is initially in a dynamic non-equilibrium state, but will over longer simulation time approach the equilibrium state.

The results are by default extracted by these algorithms and are calculated as averages over all time steps from start to finish. A suitable time frame is essential to get reliable results.

This chapter is based on the Gromacs user manual, primarily section 3.4.9 and section 8.1–8.4 [35].

3.3.1 Hydrogen Bonds

Gromacs analyzes all possibilities of hydrogen bonds between donors and acceptors. To validate a hydrogen bond a geometric criterion is used, illustrated by figure 3.1 and given by equation 3.4. The number of hydrogen bonds are calculated by the Gromacs program *gmx hbond*.

The maximal distance between a donor and an acceptor is described by r_{HB} , and the maximum value corresponds to the first minimum of the radial distribution function of a flexible water model. All existing hydrogen bonds will be found between two molecules, as described in section 2.1, or in a specified donor-hydrogen-acceptor triplet.

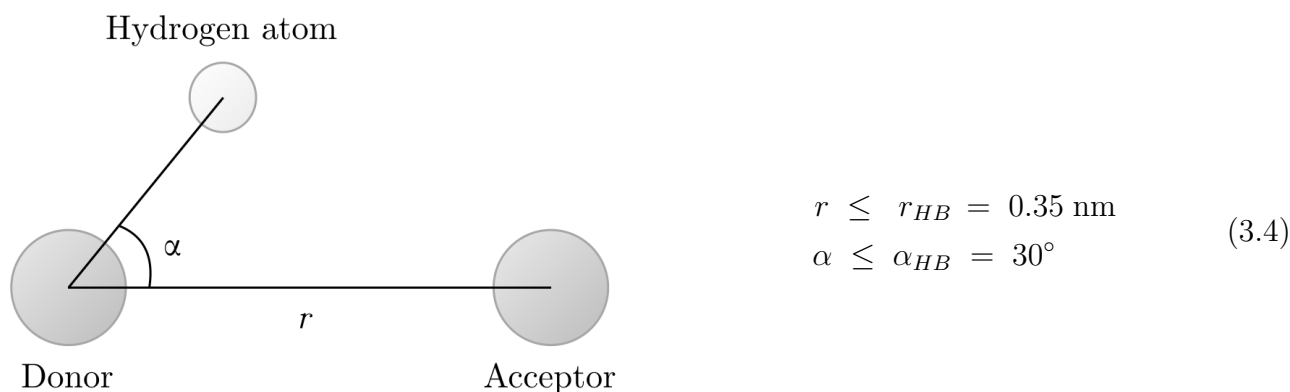


Figure 3.1: Geometric criterion for verification of the existence of a hydrogen bond.

3.3.2 Partial Density Profiles

The Gromacs program *gmx density* calculates the average mass density along one of the axis of the computational box for a chosen substance of the system. The program produces data sets that can be visualized as plots of the densities against one of the box axis. This is a useful tool when looking at the distribution of a substance over the interface in e.g. a binary mixture.

3.3.3 Radial Distribution Function

The radial distribution function (RDF) $g_{AB}(r)$ is implemented in Gromacs, and can be computed by Gromacs program *gmx rdf*. RDF gives the probability of locating a particle a from component A at a distance r from another particle b from component B in a binary mixture. RDF is defined by equation 3.5

$$4\pi r^2 g_{ab}(r) = V \sum_{i \in A} \sum_{j \in B} P(r) \tag{3.5}$$

where V is the volume of the system and $P(r)$ the probability of finding a b particle at a distance r from an a particle.

3.3.4 Energies

The systems densities, heat capacities at constant pressure, potential energies, total pressures and temperatures are all calculated by the same program, *gmx energy*. In addition, the interfacial tension in the system is also calculated by the same program, described in section 3.3.5.

The output of the energy program is chosen from a list of terms. An example of a list is shown in figure 3.2. Note that there is a wide range of different terms to choose from. The number of options is linked to the amount of different components in the system as well as when in the MD simulation the energy program is used.

1	G96Angle	2	Proper-Dih.	3	Improper-Dih.	4	LJ-14
5	Coulomb-14	6	LJ-(SR)	7	Coulomb-(SR)	8	Coul.-recip.
9	Potential	10	Kinetic-En.	11	Total-Energy	12	Temperature
13	Pressure	14	Constr.-rmsd	15	Vir-XX	16	Vir-XY
17	Vir-XZ	18	Vir-YX	19	Vir-YY	20	Vir-YZ
21	Vir-ZX	22	Vir-ZY	23	Vir-ZZ	24	Pres-XX
25	Pres-XY	26	Pres-XZ	27	Pres-YX	28	Pres-YY
29	Pres-YZ	30	Pres-ZX	31	Pres-ZY	32	Pres-ZZ
33	#Surf*SurfTen			34	Coul-SR:LUT-LUT		
35	LJ-SR:LUT-LUT			36	Coul-14:LUT-LUT		
37	LJ-14:LUT-LUT			38	Coul-SR:LUT-SOL		
39	LJ-SR:LUT-SOL			40	Coul-14:LUT-SOL		
41	LJ-14:LUT-SOL	42	Coul-SR:LUT-CL	43	LJ-SR:LUT-CL	44	Coul-14:LUT-CL
45	LJ-14:LUT-CL			46	Coul-SR:LUT-_WEO		
47	LJ-SR:LUT-_WEO			48	Coul-14:LUT-_WEO		
49	LJ-14:LUT-_WEO			50	Coul-SR:SOL-SOL		
51	LJ-SR:SOL-SOL			52	Coul-14:SOL-SOL		
53	LJ-14:SOL-SOL	54	Coul-SR:SOL-CL	55	LJ-SR:SOL-CL	56	Coul-14:SOL-CL
57	LJ-14:SOL-CL			58	Coul-SR:SOL-_WEO		
59	LJ-SR:SOL-_WEO			60	Coul-14:SOL-_WEO		
61	LJ-14:SOL-_WEO	62	Coul-SR:CL-CL	63	LJ-SR:CL-CL	64	Coul-14:CL-CL
65	LJ-14:CL-CL			66	Coul-SR:CL-_WEO		
67	LJ-SR:CL-_WEO			68	Coul-14:CL-_WEO		
69	LJ-14:CL-_WEO			70	Coul-SR:_WEO-_WEO		
71	LJ-SR:_WEO-_WEO			72	Coul-14:_WEO-_WEO		
73	LJ-14:_WEO-_WEO			74	T-LUT		
75	T-SOL	76	T-CL	77	T-_WEO	78	Lamb-LUT
79	Lamb-SOL	80	Lamb-CL	81	Lamb-_WEO		

Figure 3.2: A list of the different quantities that can be chosen from the Gromacs program *gmx energy*. The abbreviation LUT refers to 2,6-lutidine, SOL to TIP4P/2005, CL to chloride anions, and _WEO to PPh_4^+ . See the Gromacs reference manual for details of all energy terms [35].

3.3.5 Interfacial Tension

The average interfacial tension $\gamma(t)$ was calculated by Gromacs from the difference of the normal $P_N (= P_{zz}(t))$ and lateral P_L pressure in the computational box. The z-component of the pressure and the interfacial tension were coupled to a pressure bath by the Berendsen pressure coupling algorithm. $\gamma(t)$ is given by equation 3.6

$$\gamma(t) = \frac{L_z}{n} (P_N - P_L) \quad (3.6)$$

where L_z is the height of the box, n the number of surfaces, and $P_L = \frac{P_{xx}(t) + P_{yy}(t)}{2}$.

The normal pressure is corrected by scaling the height of the box with the scaling matrix element μ_{zz} shown in equation 3.7 and equation 3.8

$$\Delta P_{zz} = \frac{\Delta t}{\tau_P} (P_{0zz} - P_{zz}(t)) \quad (3.7)$$

where τ_P is the pressure time constant, P_{0zz} and $P_{zz}(t)$ is the pressure in z-direction at $t = 0$ and $t = t$ respectively, and

$$\mu_{zz} = 1 + \beta_{zz} \Delta P_{zz} \quad (3.8)$$

where β_{zz} is the isothermal compressibility of the system in z-direction. The correction of the normal pressure is used to achieve the correct convergence for the interfacial tension to the reference value γ_0 . The box length in x/y-direction is corrected by the factor $\mu_{x/y}$ given by equation 3.9

$$\mu_{x/y} = 1 + \frac{\Delta t}{2\tau_P} \beta_{x/y} \left(\frac{n\gamma_0}{\mu_{zz}L_z} - [\Delta P_{zz} + P_N - P_L] \right) \quad (3.9)$$

In the calculation of interfacial tension β_{zz} is critical since it may affect the convergence of the interfacial tension. When β_{zz} is set to zero, ΔP_{zz} is also set to zero as it is necessary to obtain the correct interfacial tension.

As mention in the previous section, the average interfacial tension is calculated by the Gromacs program *gmx energy*.

Chapter 4

MD simulations of the systems

4.1 Initial Composition of Water/2,6-Lutidine System

To illustrate the interface between water and 2,6-lutidine, the volume of the two phases is initially set to be equal. This means that the initial volume of the system is half water and half 2,6-lutidine. With this being said, this does not mean the system consists of 50 mol% water and 50 mol% 2,6-lutidine, as the 2,6-lutidine molecules are larger than the water molecules. The system consists of many more water molecules than 2,6-lutidine molecules. If figure 2.1a and figure 2.3a is compared, it obvious that a 2,6-lutidine molecule has a larger volume than a water molecule. This results in the initial composition of 86.36 mol% water and 13.64 mol% 2,6-lutidine, where the water and 2,6-lutidine phases obtains equal volumes.

The phase diagram of water and 2,6-lutidine is shown in figure 4.1. The systems in this thesis are given in mol% (as shown in table 4.1) so to compare the initial system to figure 4.1, the mole percent of 2,6-lutidine was converted to mass fraction by equation 4.1, as described by Pousaneh et al.

$$w_l = \frac{x_l}{x_l + (1 - x_l)\left(\frac{M_w}{M_l}\right)} \quad (4.1)$$

where w_l is mass fraction of 2,6-lutidine, x_l mole fraction of 2,6-lutidine, and M_w and M_l molar masses of water and 2,6-lutidine [47]. Point P in figure 4.1 marks the initial composition of the system with 0 mol% PPh₄Cl at $T_{sim} = 380$ K.

Pousaneh et al. obtained $T_{LCP,sim}$ from simulated density profiles to $T_{LCP,sim} = 310.5 \pm 1.5$ K. Even though this is a couple of degrees higher than the experimental temperature at $T_{LCP} = 307.15$ K [14], $T_{LCP,sim}$ is valid for the work in this thesis as the system simulated by Pousaneh et al. uses the same water and 2,6-lutidine model. The simulated value of $T_{UCP,sim}$ by Pousaneh et al. is found between 450 and 510 K, which is in the upper part of the phase diagram of water/2,6-lutidine.

As this thesis studies interfacial tension at the interface between water and 2,6-lutidine, it is essential that an interface exists. To obtain an interface the initial system needs to be found

inside the miscibility gap. In order to have phase separation, the volumes of water and 2,6-lutidine are requested to be equal. It is necessary that the temperature is between $T_{LCP,sim} = 310.5 \pm 1.5$ K and $T_{UCP,sim} = 450$ K and that the mass fraction of 2,6-lutidine sets the systems to the miscibility gap. With this in mind, the simulation temperature T_{sim} is set to 380 K. All systems were simulated to T_{sim} by thermostats.

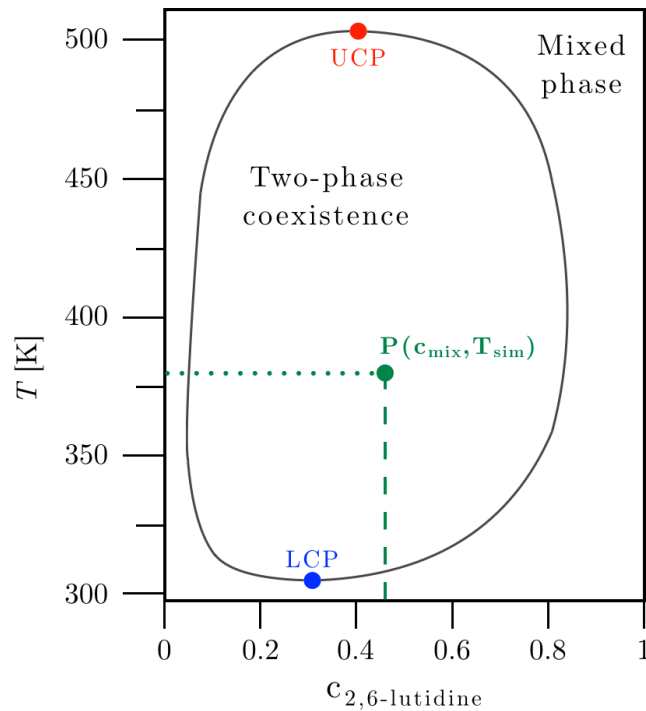


Figure 4.1: Illustration of the bulk phase diagram of water/2,6-lutidine system at constant volume. $C_{2,6-lutidine}$ denotes mass fraction of 2,6-lutidine. UCP and LCP indicates the upper and the lower critical point, describing the outline of the coexistence loop [14]. The green - - line indicates mass fraction of 2,6-lutidine of the initial system, and the green $\cdot\cdot$ line indicates the simulation temperature $T_{sim} = 380$ K for all systems. Point P indicates where the the two lines intercept, and where the initial system is located.

4.2 MD Simulations with Gromacs

The basics of performing MD simulations with Gromacs can be described with five steps, outlined in figure 4.2. The description of the different steps is mainly based on the Gromacs reference manual [35], and the virtual simulation seminar "Molecular Dynamics Simulations with Gromacs" given by Aleksandar Mehandzhiyski [33]. All Gromacs programs mentioned are described in appendix B, and Gromacs files in A.8 and C. For further details see the Gromacs reference manual [35].

Step 1: Preparation of the systems

The first step involves defining all chemical components and the amount of each component, with Gromacs program *gmx insert-molecules*. In MD simulations the systems are simulated inside a space-filling computational box, surrounded by rendered copies of itself. See appendix A.1 for more about periodic boundary conditions. The required amount of each component that together represents the system, are added to the computational box. The system can be scaled through *gmx editconf*. It is important that all molecules fit inside the box, but also that the box is not too large. A too large box can cause problems in step 4. If the system consist of water, an amount of a water model can be added to the box by *gmx solvate*. The system is validated by *gmx grompp*. If charged solute is added, e.g. PPh_4^+ , ions are required to be added as well by *gmx genion*, e.g. Cl^- [28]. All parameters for the simulation are stated through parameter files.

Step 2: Energy Minimization

Initially, a system can be far from equilibrium with large forces that often leads to failure of MD simulations. Energy minimization is therefore necessary to remove excess energy, and to reduce the prospect of failure. Energy minimization is the process where atoms are rearranged so net inter-atomic forces on each atom is acceptably close to zero, and sets the potential energy surface at a fixed point. The first step of minimizing energy is to check the topology file by *gmx grompp*. The minimization is completed by Gromacs main computational chemistry engine *gmx mdrun* with parameters from the parameter file for the minimization.

The minimization is confirmed by analyzing graphs for different energies of the system, by *gmx energy*. Data sets for plotting graphs are also computed by *gmx energy*. If it seems like the energy is not minimized, another energy minimization should be conducted and/or the minimization should be extended and/or the parameters for the minimization should be reviewed.

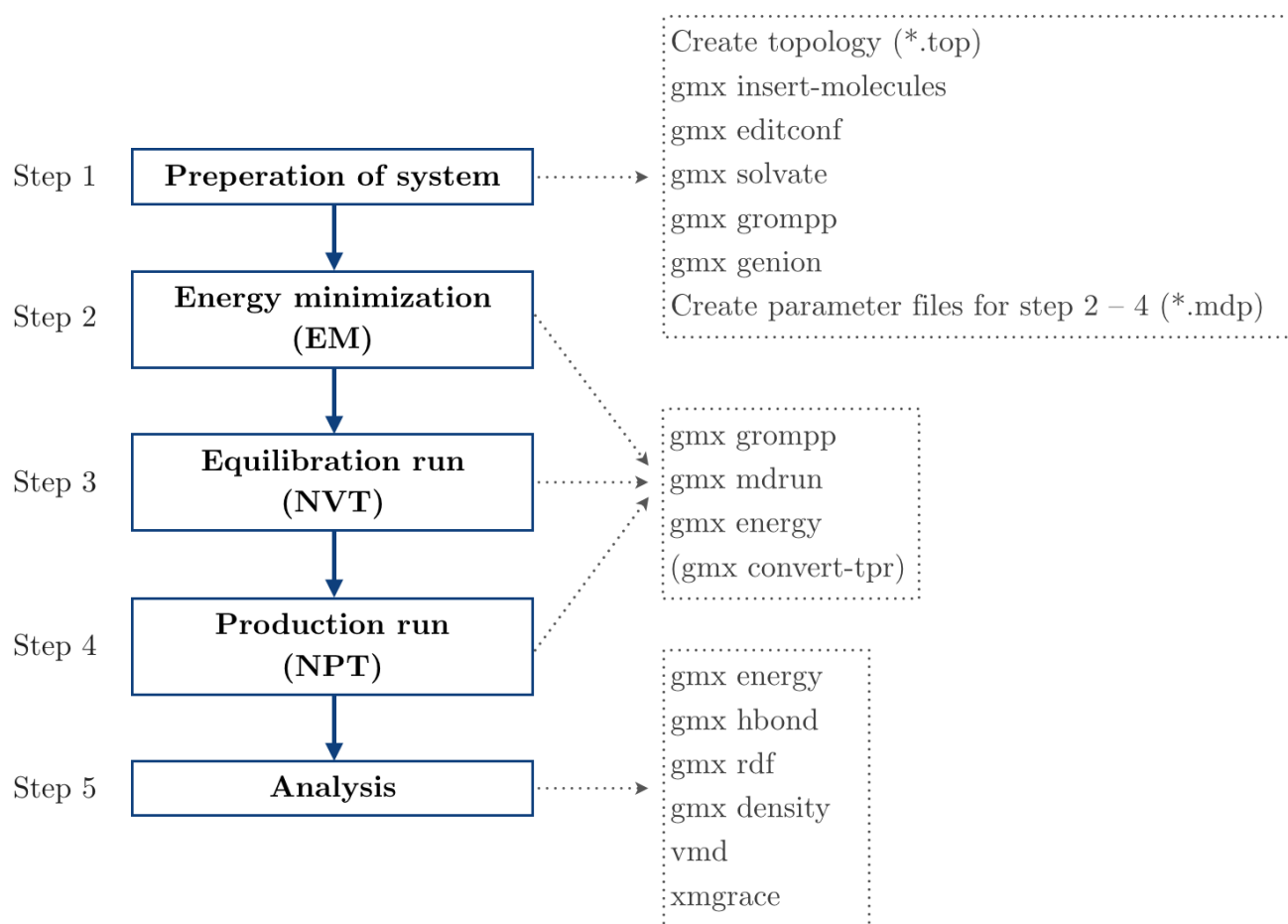


Figure 4.2: Outline of a MD simulation by Gromacs [33]. Each step is connected to a dotted box that describes which Gromacs programs run, which files created, and additional programs that are run to fulfill each step.

Step 3: Equilibration run

The systems in this thesis will be equilibrated over time t by the canonical ensemble (NVT), where the number of particles (N), volume (V), and temperature (T) are simulated to constant values. A system needs to be equilibrated, but not necessarily by NVT. The purpose of doing a NVT simulation before the production run, is to get a reasonable velocity distribution. The equilibration run is again simulated by Gromacs main computational chemistry engine *gmx mdrun* with parameters from the parameter file for NVT. The topology file for the system are checked in advance by *gmx grompp*. If the simulation time is too short to obtain an equilibrated system, the simulation time can be extended by *gmx convert-tpr*.

The equilibration of the system is confirmed by again analyzing graphs for different energies of the system as well as hydrogen bonds, partial density profiles etc., and the graphs are used to confirm that the system goes towards equilibrium. Energy components are extracted by *gmx energy*, as well as the data sets used for plotting graphs.

Step 4: Production run

By obtaining a reasonable velocity distribution by NVT, NPT is performed to obtain the correct density of the system. In a NPT simulation, a simulation with the isothermal-isobaric ensemble, the number of particles (N), pressure (P), and temperature (T) are simulated to constant values. A MD simulation needs a production step, but not necessarily by NPT. The production run produces the data sets analyzed in step 5, by *gmx mdrun* with parameters from the parameter file for NPT. The topology file is checked in advance by *gmx grompp*. If the simulation time is again too short, the simulation time can be extended by *gmx convert-tpr*.

In the previous steps the volume of a system were simulated to be constant. During NPT simulations the volume of the system will shrink into a more fitting size. If the box is too large compared to the system, the simulation may blow up, meaning that the the simulation fails. Therefore the configuration of the box size done in step 1 is essential to avoid eventual failures during step 4.

Step 5: Analysis

Before an analysis can be commenced and completed, the state of the system has to be checked. It is necessary that the system is at equilibrium. The equilibrated state is confirmed by studies of different quantities through graphical presentations. In MD simulations structural analysis, such as radial distribution functions, density profiles, and hydrogen bonds needs to be completed, as well as studies of different energies. When the equilibrium state is confirmed, the analysis can start.

The system produced at step 4 is analyzed as the final step of a MD simulation. A variety of energies are extracted by *gmx energy*, information about hydrogen bonds by *gmx hbond*, radial distribution function by *gmx rdf*, and density profiles by *gmx density*. All four programs were studied in section 3.3.

By default the results of *gmx energy*, *gmx hbond*, *gmx rdf*, and *gmx density* are calculated as averages over all time steps from start to finish. Reliable results are calculated from where the

system reaches equilibrium, and naturally ends when the simulation stops. The starting time is defined by studying a variety of graphs for different energies, such as pressure, temperature, potential energy, and volume, as well as studying graphs presenting radial distribution functions, density profiles, and hydrogen bonds. All of these quantities need to be studied thoroughly before a suitable start time can be decided.

Graphs are plotted with Grace by command *xmgrace*, a free plotting tool that plots two-dimensional numerical data with many possibilities to compute suitable plots [64]. To produce molecular figures VMD (Visual molecular dynamics) can be used by command *vmd* [21].

4.3 Preparation

To prepare all systems for simulations, a water/2,6-lutidine system without PPh₄Cl was made. Then the remaining six systems were created from the first system with additions of different concentrations of PPh₄Cl.

4.3.1 Water/2,6-Lutidine System

To have flat interfaces in the water/2,6-lutidine system, it is necessary to fill the volume of the box with equal volumes of water and 2,6-lutidine. The total amount of molecules in the system needs to be calculated. A too large system will need too large computing power and takes too long time to simulate. A too small system will give unrealistic results. Thus the system was composed of 3 000 2,6-lutidine model molecules. TIP4P/2005 molecules are smaller than 2,6-lutidine molecules by a factor of $\frac{19}{3} \approx 6.33$. The equivalent volume of water was 19 000 TIP4P/2005 molecules [47].

Energy Minimization

For the energy minimization (step 2 in section 4.2) the GROMOS 45A7 force field was applied for Lennard-Jones pair potential parameters and bond lengths. A cut-off length of 1.2 nm was applied for Lennard-Jones interactions, which is a good choice for molecular sizes in this thesis. A plain cut-off with neighborlist radius of 1.2 nm was applied for the Coulomb type, as long-range electrostatic interactions were present. For neighbour searching the Verlet cut-off scheme was used. The energy of the system was minimized for 3.36 ns with an initial step size of 0.001 nm. The parameter file for the energy minimization of water/2,6-lutidine is found in appendix C.1.1.

Equilibration and Production Run

For the following steps, described as step 3 and 4 in section 4.2, the GROMOS 45A7 force field was applied for the Lennard-Jones parameters. A cut-off length of 1.2 nm was applied as the cut-off length for short-range neighbour list, distance for the Coulomb cut-off, and distance for

Lennard-Jones cut-off. Fast smooth Particle-Mesh Ewald (PME) electrostatics were applied for the Coulomb interactions, as long-range electrostatic interactions were present. All bond lengths were constrained with the LINCS algorithm.

The system was equilibrated through 185 ns with an initial step size of 0.002 ps. The temperature was coupled to the Berendsen thermostat with $T_{sim} = 380$ K. No pressure coupling was applied for this step of the simulation, as the equilibration run operates under NVT. Velocities were generated according to the Maxwell distribution. The parameter file for the equilibration run of water/2,6-lutidine is found in appendix C.1.2.

After NVT the system was simulated for analysis through 286 ns with an initial step size of 0.002 ps. The temperature was coupled to the Velocity-rescaling thermostat with $T_{sim} = 380$ K. As the production run operates under NPT, the pressure of the system was coupled to the Parrinello-Rahman barostat with reference pressure $p_{sim} = 1$ bar. This means that after the production run the volume of the system will change, as seen by the graph in figure 5.1d. The development of five other quantities for the equilibrated system can be found in the same figure. The parameter file for the equilibration run of water/2,6-lutidine is found in appendix C.1.3.

4.3.2 Water/2,6-Lutidine System with PPh₄Cl

Six systems were produced by adding different concentrations of PPh₄Cl to the already equilibrated water/2,6-lutidine system. The compositions of the systems are given in table 4.1, described by number of molecules and mole percent. The additions of PPh₄Cl were completed as described in step 1 in section 4.2. Before energy minimizations the initial box sizes were confirmed to be large enough for the different amounts of molecules for the six systems.

Energy Minimization

The process of reducing the energy in the different systems, was completed following the process described in step 2 in section 4.2. The parameter file for energy minimization is seen in appendix C.2.1.

Energy minimizations were completed with the GROMOS 45A7 force field for Lennard-Jones pair potential parameters and bond lengths. A cut-off length of 1.2 nm was applied for Lennard-Jones interactions. A plain cut-off with neighborlist radius of 1.2 nm was applied for the Coulomb type, as long-range electrostatic interactions were present. For neighbour searching the Verlet cut-off scheme was used. Fast smooth Particle-Mesh Ewald (PME) was applied for the Coulomb interactions for long-range electrostatic interactions. The energies of the systems were minimized with an initial step size of 0.001 nm.

Table 4.1: Overview of the seven systems simulated, composed of the antagonistic salt PPh₄Cl, water, and the organic solvent 2,6-lutidine (C₇H₉N). The concentrations of the components are expressed by the number of molecules and by mol%.

Number of molecules			Mole percent (mol%)		
PPh ₄ Cl	water	2,6-lutidine	PPh ₄ Cl	water	2,6-lutidine
0	19 000	3 000	0.00	86.36	13.64
10	18 990	3 000	0.05	86.31	13.64
30	18 970	3 000	0.14	86.22	13.64
60	18 940	3 000	0.27	86.09	13.64
80	18 920	3 000	0.36	86.00	13.64
100	18 900	3 000	0.45	85.91	13.64
300	18 700	3 000	1.36	85.00	13.64

4.4 MD Simulations

The system with 0.00 mol% PPh₄Cl was generated in section 4.3.1. This section goes through the equilibration and production run for the remaining six systems, based on section 4.3.2. The systems were completed according to step 3 and 4 in section 4.2.

For the equilibration and production run, the GROMOS 45A7 force field was applied for Lennard-Jones parameters. A cut-off length of $r_c = 1.2$ nm was applied for Lennard-Jones interactions. Fast smooth Particle-Mesh Ewald electrostatics were applied for the Coulomb interactions, as long-range electrostatic interactions were present. All bond lengths were constrained with the LINCS algorithm. The initial step size for both equilibration and production run was set equal to 0.002 ps. Total simulation lengths are shown in table 4.2.

Equilibration Run

The temperature was coupled to the Berendsen thermostat with reference temperature equal to 380 K. There was no change in pressure and no pressure coupling applied for this step of the simulation, as the equilibration run operates under NVT. The volume of the box was in other words constant. Velocities were generated according to the Maxwell distribution. The parameter file for the equilibration run of water/2,6-lutidine with salts is found in appendix C.2.2.

Production Run

The temperature was coupled to the Velocity-rescaling thermostat with $T_{sim} = 380$ K. As the production run operates under NPT, the pressure of the system was coupled to the Parrinello-Rahman barostat with $p_{sim} = 1$ bar. This means that after the production run, compared to the equilibration run, the volume of the box changed. The parameter file for the equilibration run of water/2,6-lutidine with salts is found in appendix C.2.3.

Table 4.2: Overview of the time lengths for the simulations for all seven systems. NVT indicates the length of simulation by canonical ensemble, and NPT by isothermal-isobaric ensemble.

mol% PPh ₄ Cl	Simulation length	
	NVT	NPT
0	185 ns	286 ns
0.05	159 ns	266 ns
0.14	154 ns	254 ns
0.27	161 ns	254 ns
0.36	154 ns	257 ns
0.45	162 ns	300 ns
1.36	200 ns	276 ns

Chapter 5

Results

Section 5.1 describes how the results were extracted, generated and rendered, before the rest of this chapter presents the simulated results. The following results are chosen as they give a base to explain how the concentration of PPh₄Cl influence the interfacial tension of a water/2,6-lutidine system.

5.1 Analysis

First the systems were confirmed to be at equilibrium by graphical presentations as explained in step 5 in section 4.2. Figure 5.1 presents time evaluation of six different quantities for the system with 0.00 mol% PPh₄Cl. As the simulation goes by, the systems stabilizes and the equilibrium state is reached as seen in the graphs as stabilization of the curves.

Molecular configurations of all systems were rendered from the final simulations, shown in section 5.2.

As the Gromacs programs calculates averages for the whole simulation, all calculations are computed over individual time frames. Start times were based on thorough studies of a variety of graphs as described in step 5. A suitable start time was set to 150 ns, and the time frames ended as stated in 4.2. The calculations of interfacial tension were calculated for the following time frames, all starting at 25 ns and ending for 0.00 mol% to 1.36 mol% PPh₄Cl, in ascending order 70 ns, 132 ns, 146 ns, 142 ns, 145 ns, 140 ns, and 141 ns.

The number of hydrogen bonds were calculated by Gromacs program *gmx hbond*, density profiles by *gmx density*, and radial distribution function by *gmx rdf*, as described in section 3.3. Temperature, pressure, density, heat capacity at constant pressure, and potential energy were extracted with Gromacs program *gmx energy*. The results are shown in table 5.1. To obtain interfacial tension of the systems by *gmx energy*, MD simulations with NPT were re-run with Berendsen barostat, as described in section 3.3.5.

Density, potential, hydrogen bonds for 2,6-lutidine in the system, and interfacial tension for all system as functions of time, are shown in section 5.4. Section 5.3 shows partial density profiles for the systems with 0.00 mol%, 0.14 mol%, 0.36 mol%, and 1.36 mol% PPh₄Cl.

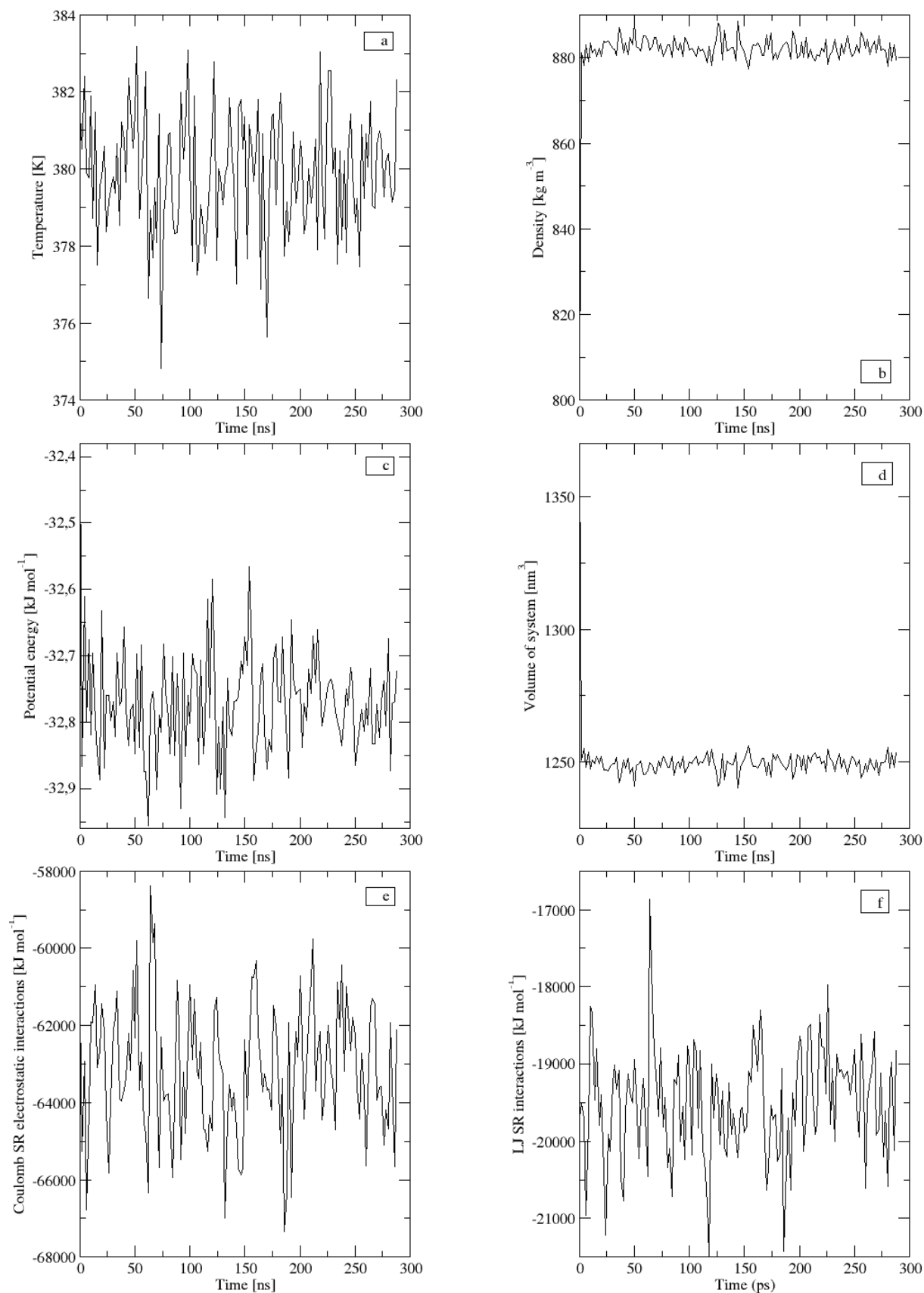


Figure 5.1: Quantities during production run for the water/2,6-lutidine system with 0.00 mol% PPh_4Cl . Graph (a) is of temperature, (b) density, (c) potential energy per molecule, (d) volume, (e) Coulomb short range electrostatic interactions, and (f) short range intramolecular LJ interactions.

5.2 Molecular Configurations

Figure 5.2 – 5.8 shows the final molecular configurations of the seven systems outlined in table 4.1. All configurations were rendered as section 5.1 describes.

In figure 5.2 – 5.8 water molecules are illustrated by blue points and 2,6-lutidine molecules by orange. Hydrophilic anions Cl^- are illustrated by green spheres, and hydrophobic cations (PPh_4^+) by dark orange spheres. The size difference of the four components are not true to size, as the design is chosen to highlight the interfaces as well as the positions of the ions.

The interfaces between water and lutidine are in the x/y-plane, and box length in z-direction. This applies to all of the molecular configurations.

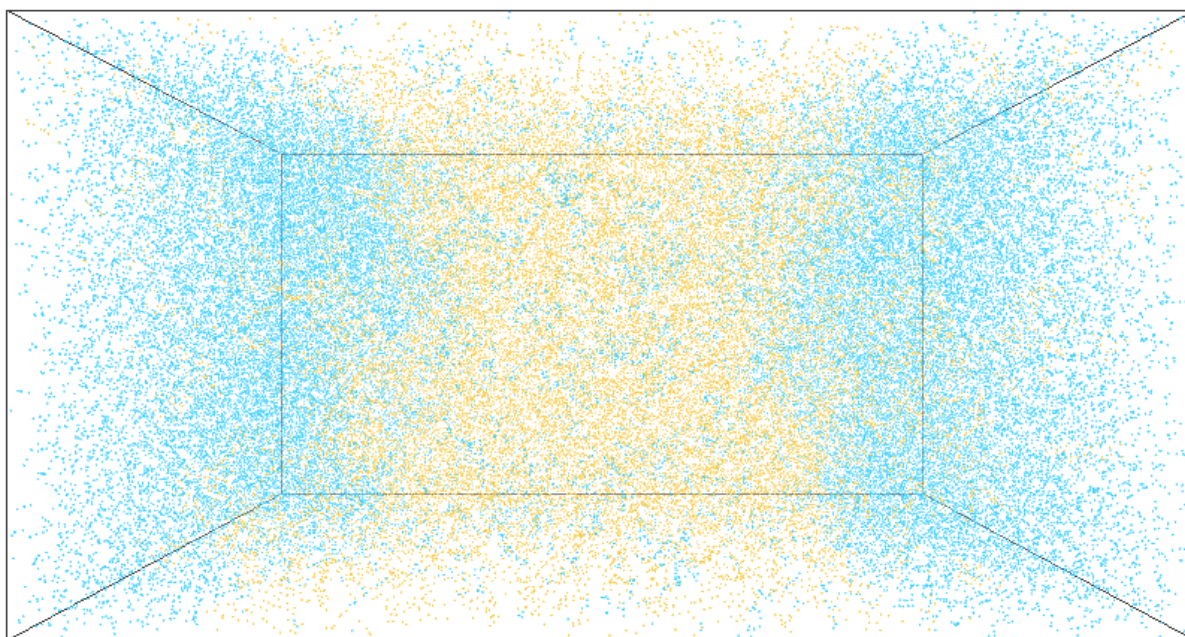


Figure 5.2: Molecular configuration of the water/2,6-lutidine system with 0.00 mol% PPh_4Cl after 286 ns of NPT simulation. Blue points indicate water and orange 2,6-lutidine.

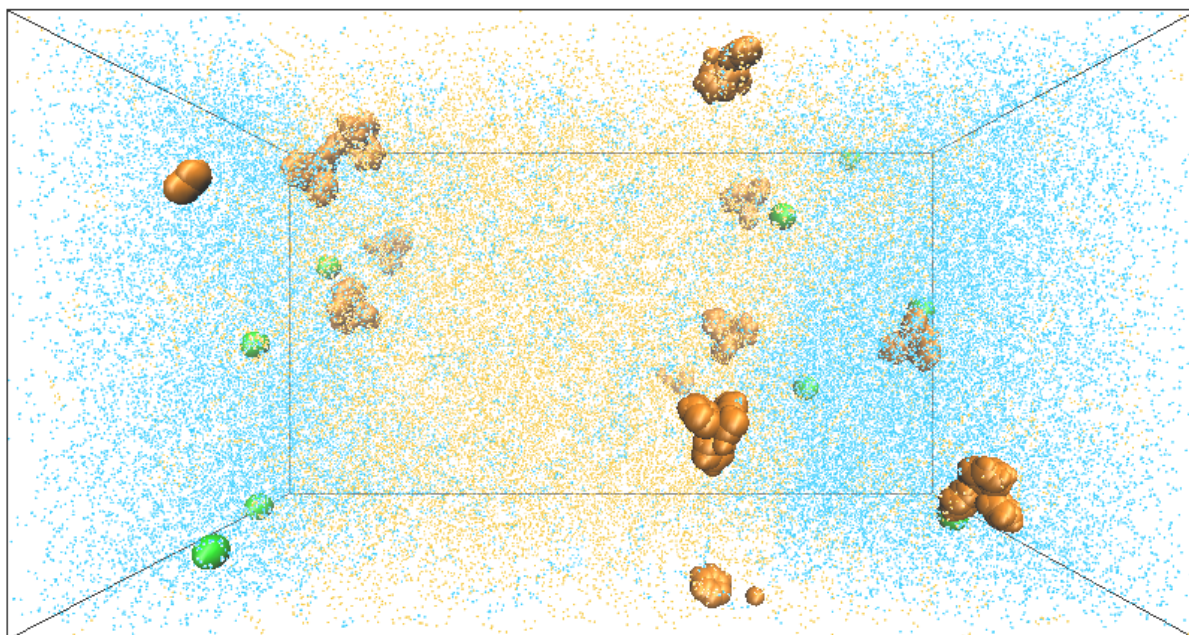


Figure 5.3: Molecular configuration of the water/2,6-lutidine system with 0.05 mol% PPh₄Cl after 266 ns of NPT simulation. Blue points indicate water and orange 2,6-lutidine. Green spheres illustrates Cl⁻ anions and orange spheres PPh₄⁺ cations.

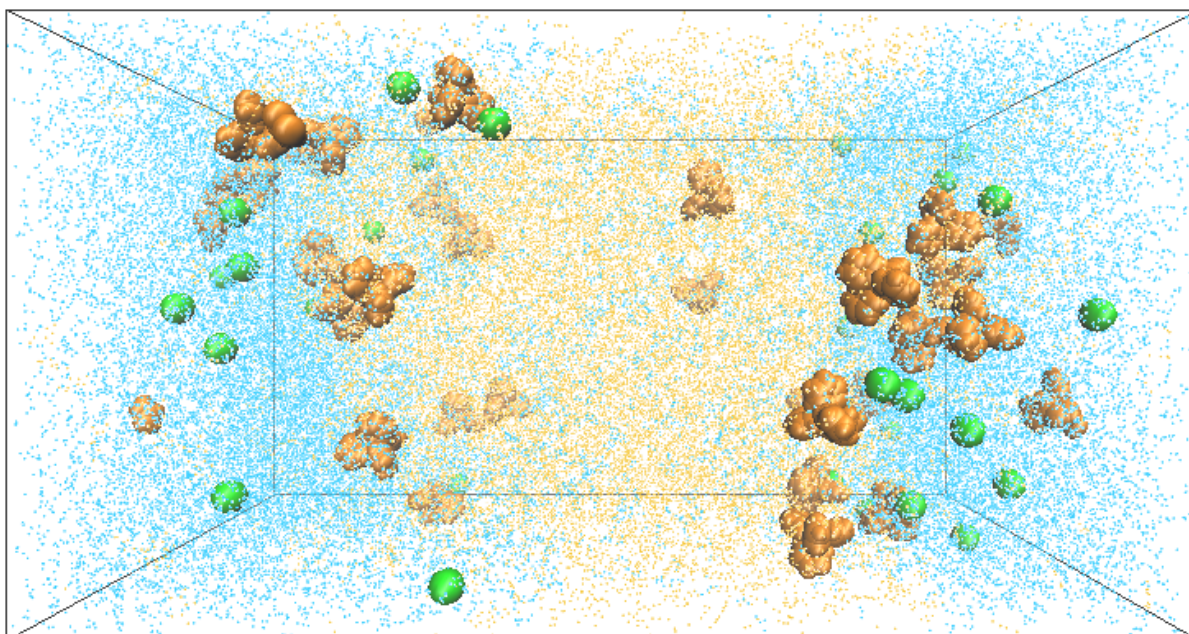


Figure 5.4: Molecular configuration of the water/2,6-lutidine system with 0.14 mol% PPh₄Cl after 254 ns of NPT simulation. Blue points indicate water and orange 2,6-lutidine. Green spheres illustrates Cl⁻ anions and orange spheres PPh₄⁺ cations.

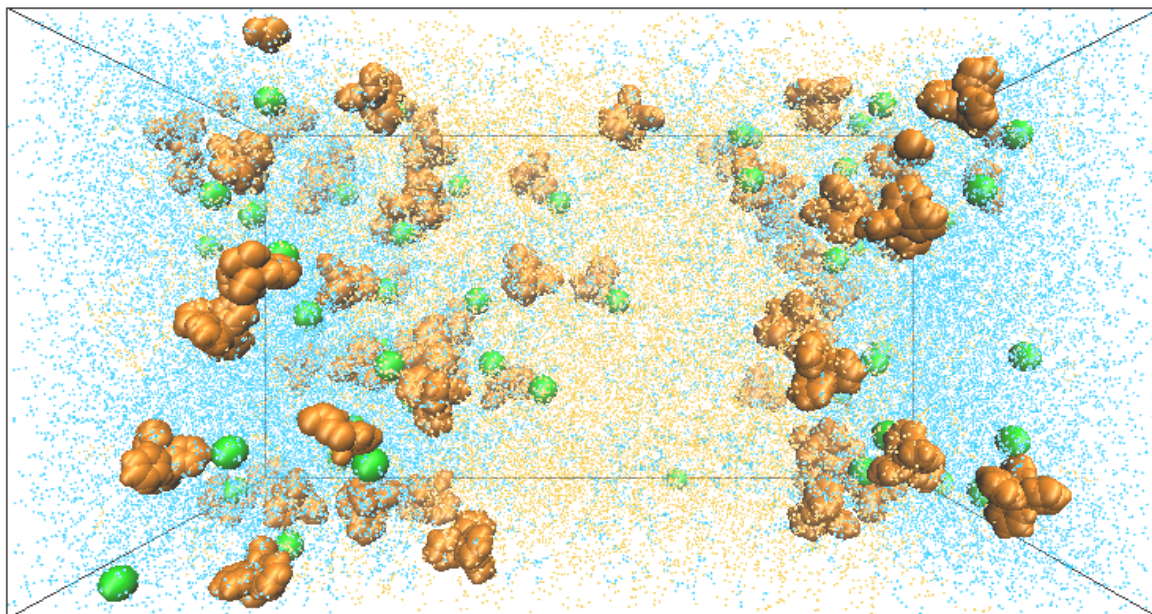


Figure 5.5: Molecular configuration of the water/2,6-lutidine system with 0.27 mol% PPh₄Cl after 254 ns of NPT simulation. Blue points indicate water and orange 2,6-lutidine. Green spheres illustrates Cl⁻ anions and orange spheres PPh₄⁺ cations.

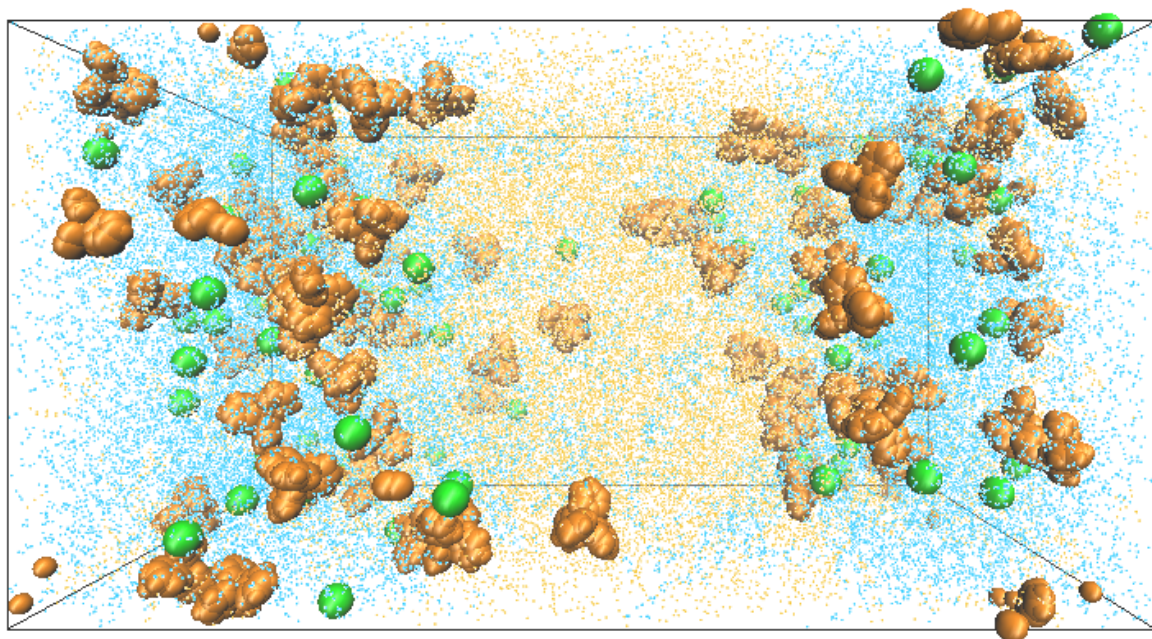


Figure 5.6: Molecular configuration of the water/2,6-lutidine system with 0.36 mol% PPh₄Cl after 257 ns of NPT simulation. Blue points indicate water and orange 2,6-lutidine. Green spheres illustrates Cl⁻ anions and orange spheres PPh₄⁺ cations.

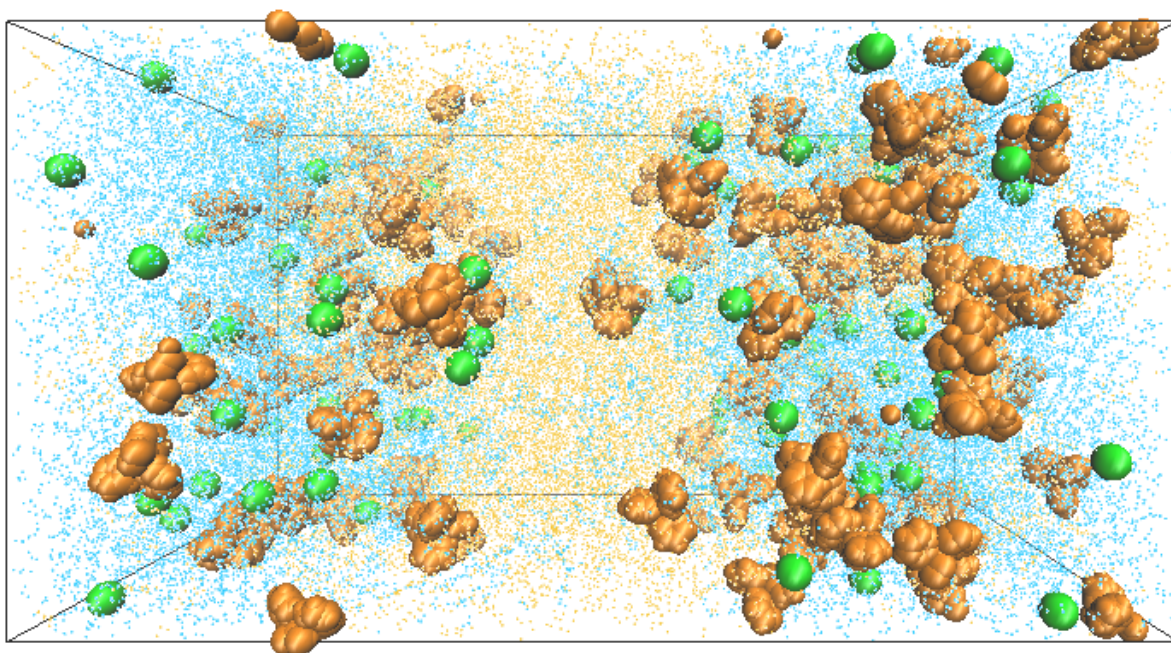


Figure 5.7: Molecular configuration of the water/2,6-lutidine system with 0.45 mol% PPh₄Cl after 300 ns of NPT simulation. Blue points indicate water and orange 2,6-lutidine. Green spheres illustrates Cl⁻ anions and orange spheres PPh₄⁺ cations.

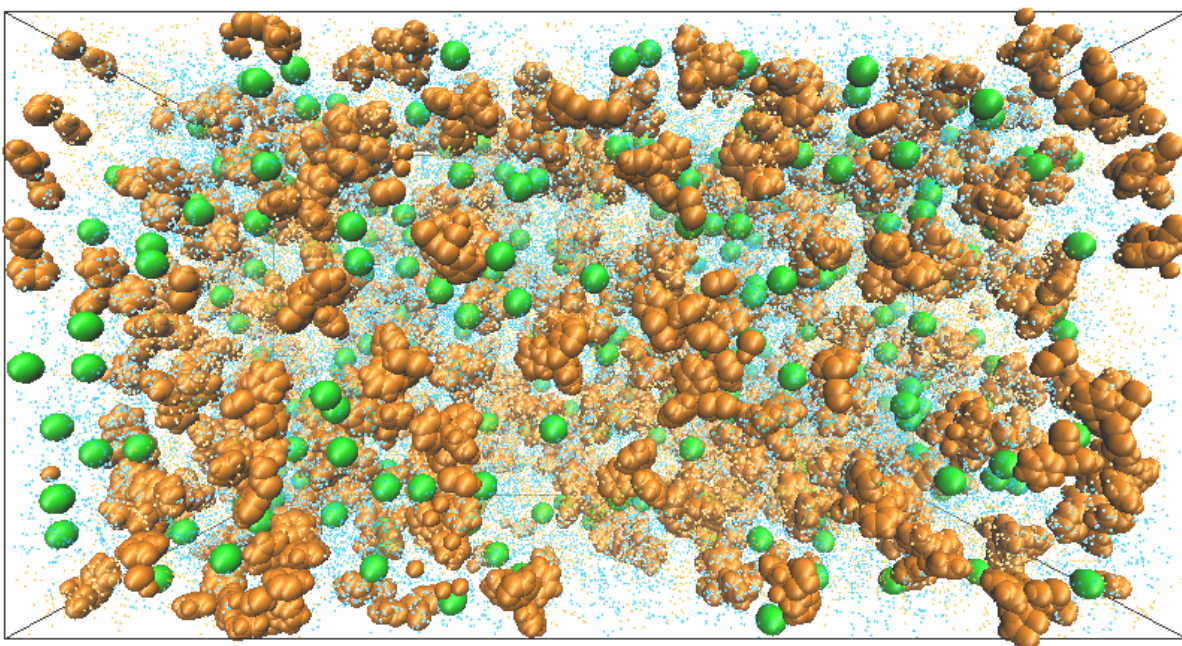


Figure 5.8: Molecular configuration of the water/2,6-lutidine system with 1.36 mol% PPh₄Cl after 2760 ns of NPT simulation. Blue points indicate water and orange 2,6-lutidine. Green spheres illustrates Cl⁻ anions and orange spheres PPh₄⁺ cations.

5.3 Partial Density Profiles

Average partial density profiles across the following four systems in z-direction: 0.00 mol%, 0.14 mol%, 0.36 mol%, and 1.36 mol% PPh₄Cl. The profiles were calculated from 150 ns to 286 ns, 254 ns, 257 ns, and 276 ns, respectively, after equilibrium averaging.

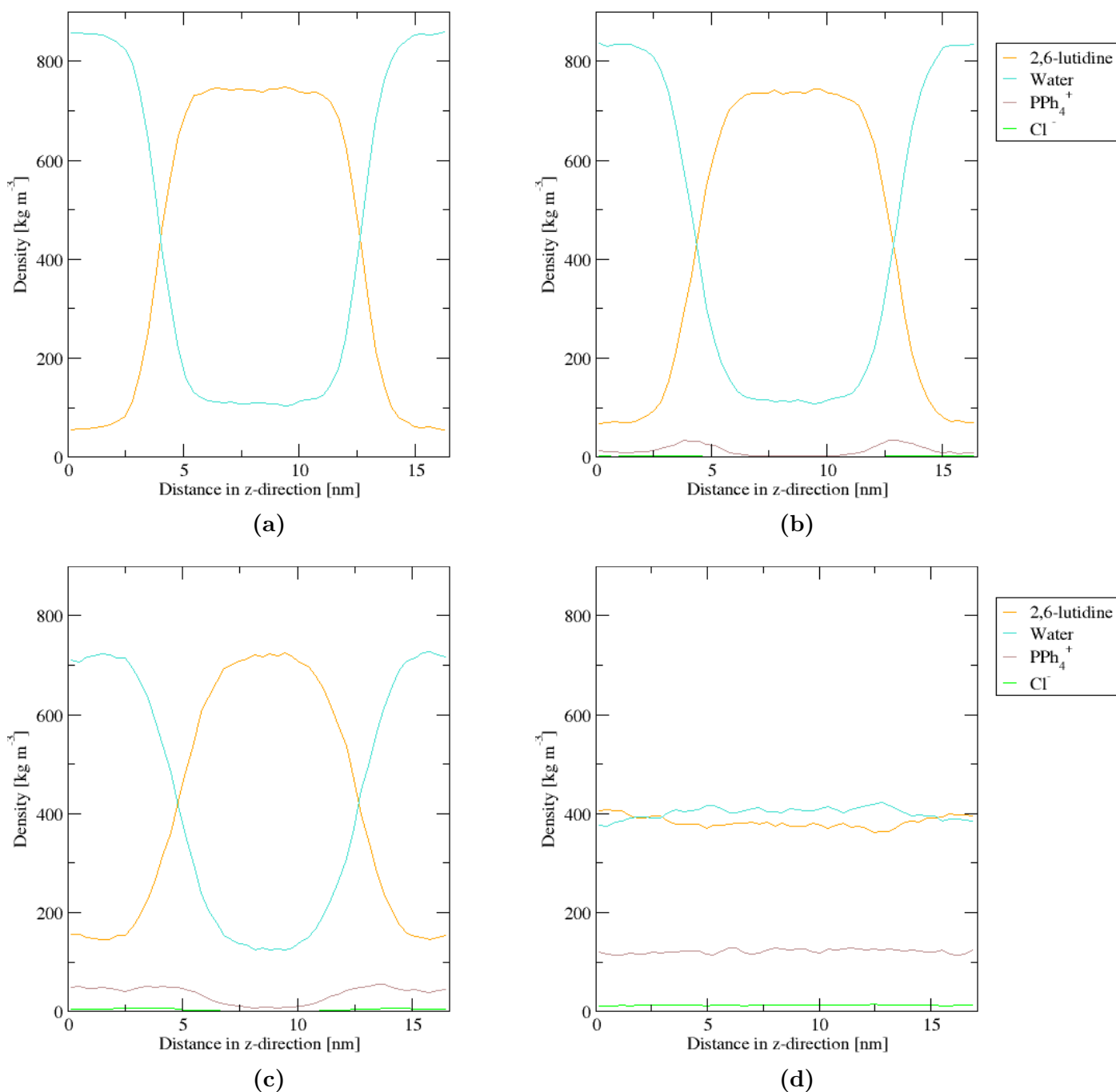


Figure 5.9: Density profile of the water/2,6-lutidine system with (a) 0.00 mol%, (b) 0.14 mol%, (c) 0.36 mol%, and (d) 1.36 mol% PPh₄Cl averaged over time from 150 ns to 286 ns, 254 ns, 257 ns, and 276 ns respectively.

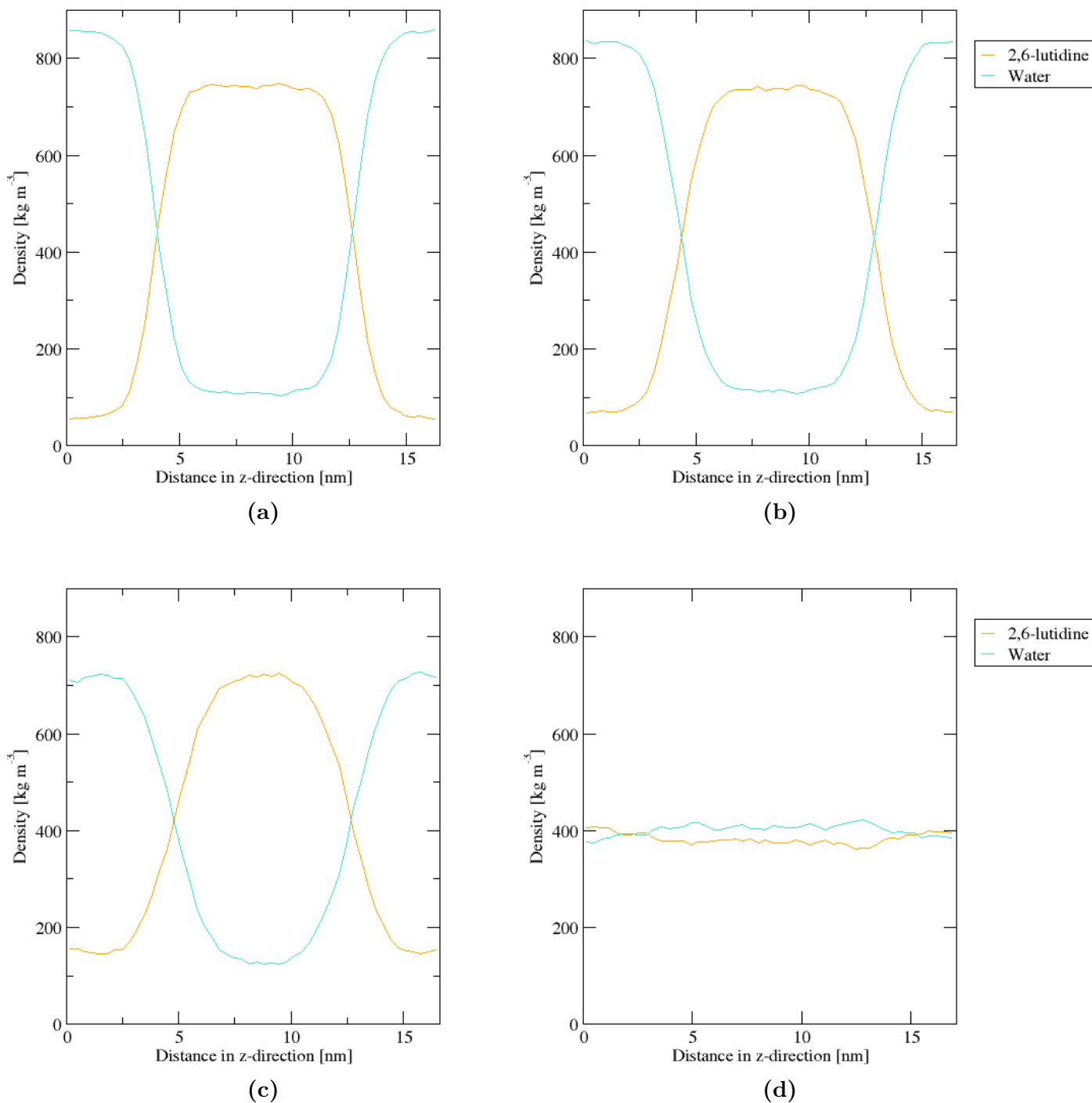


Figure 5.10: Density profile of water and lutidine in the water/2,6-lutidine system with (a) 0.00 mol%, (b) 0.14 mol%, (c) 0.36 mol%, and (d) 1.36 mol% PPh₄Cl averaged over time from 150 ns to 286 ns, 254 ns, 257 ns, and 276 ns respectively.

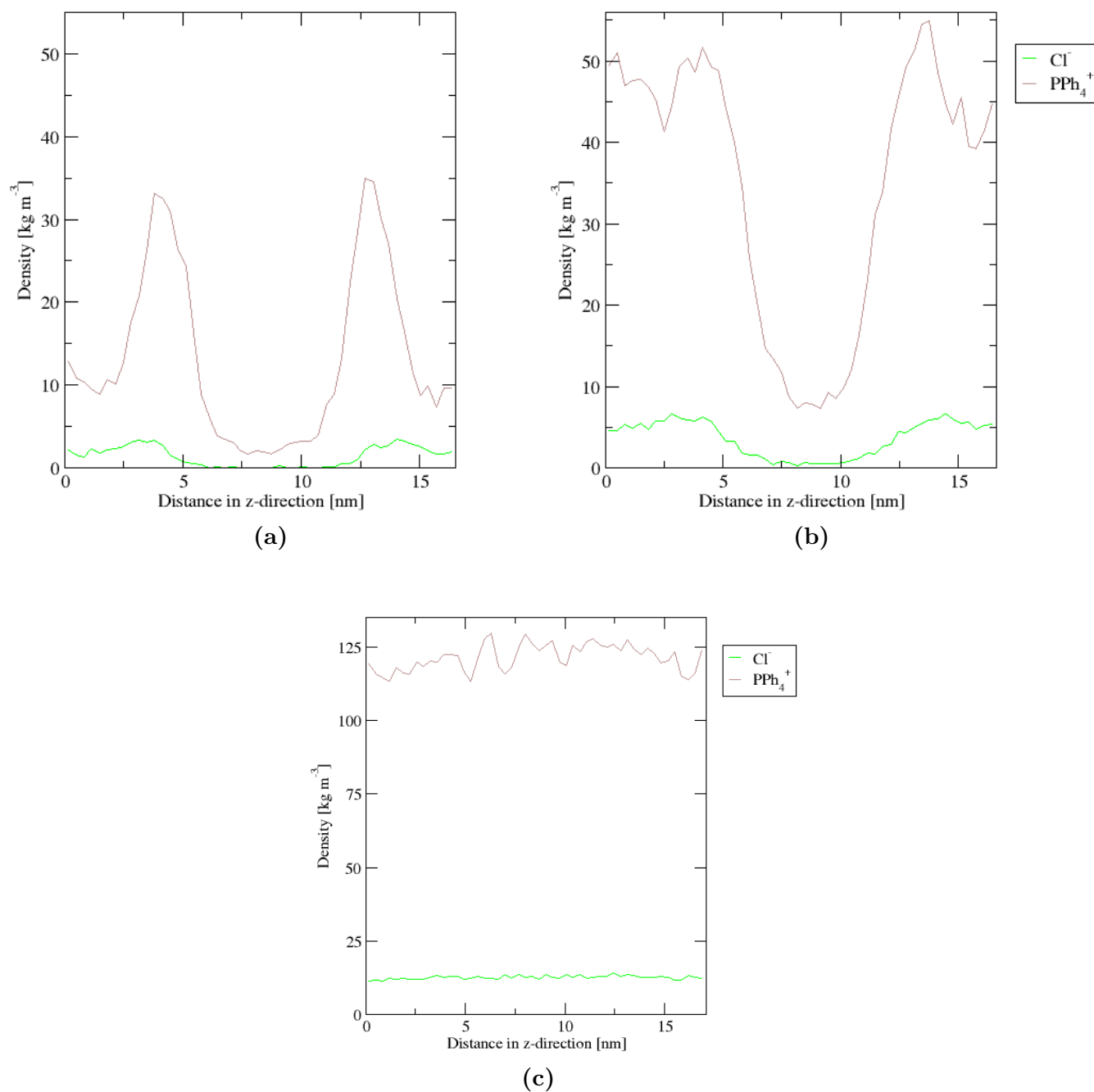


Figure 5.11: Density profile of hydrophobic cations PPh_4^+ and hydrophilic anions Cl^- in the water/2,6-lutidine system with (a) 0.14 mol%, (b) 0.36 mol%, and (c) 1.36 mol% PPh_4Cl averaged over time from 150 ns to 286 ns, 254 ns, 257 ns, and 276 ns respectively.

5.4 Graphical Representation of Results

Figure 5.12 – 5.15 represent four different quantities: density, potential energy, number of hydrogen bonds between 2,6-lutidine and water, and interfacial tension for the systems. All data were extracted from an equilibrated state of the systems.

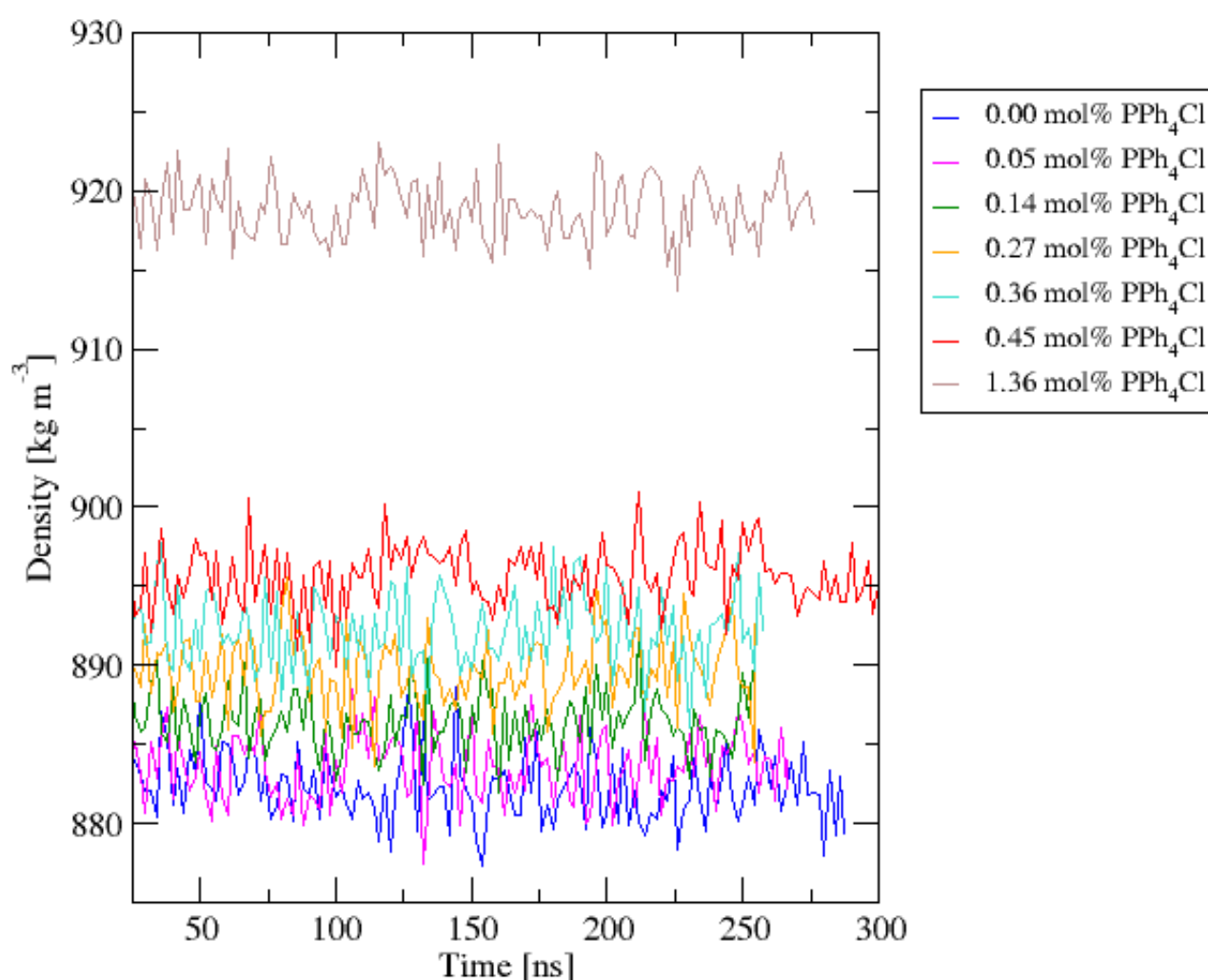


Figure 5.12: Total density $\rho(t)$ of the water/2,6-lutidine system with different mol% of PPh₄Cl, from 25 ns of simulation with NPT at $T_{sim} = 380$ K and $p_{sim} = 1$ bar.

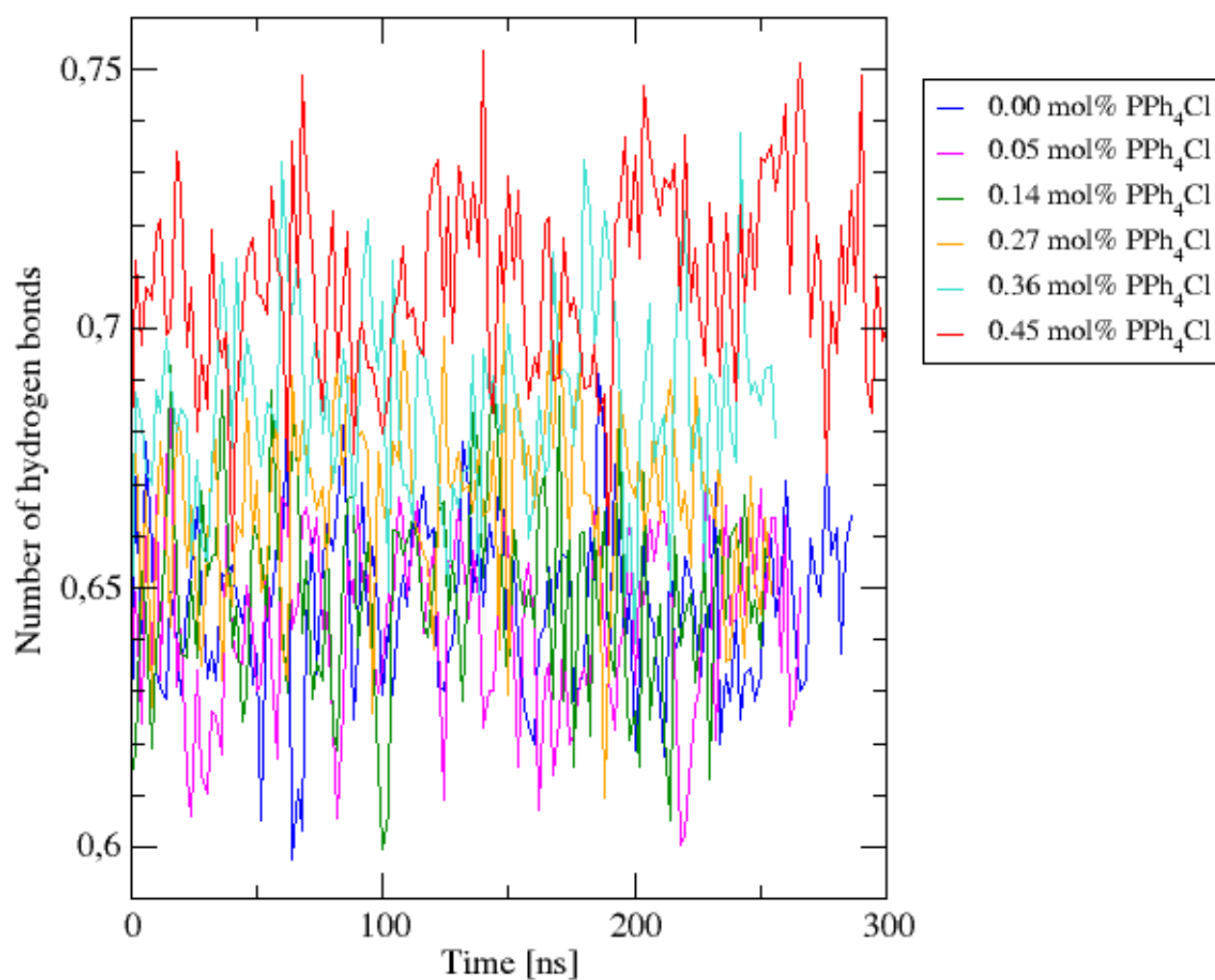


Figure 5.13: Number of hydrogen bonds between water and 2,6-lutidine per 2,6-lutidine molecule for all systems with different mol% of PPh₄Cl at $T_{sim} = 380$ K and $p_{sim} = 1$ bar.

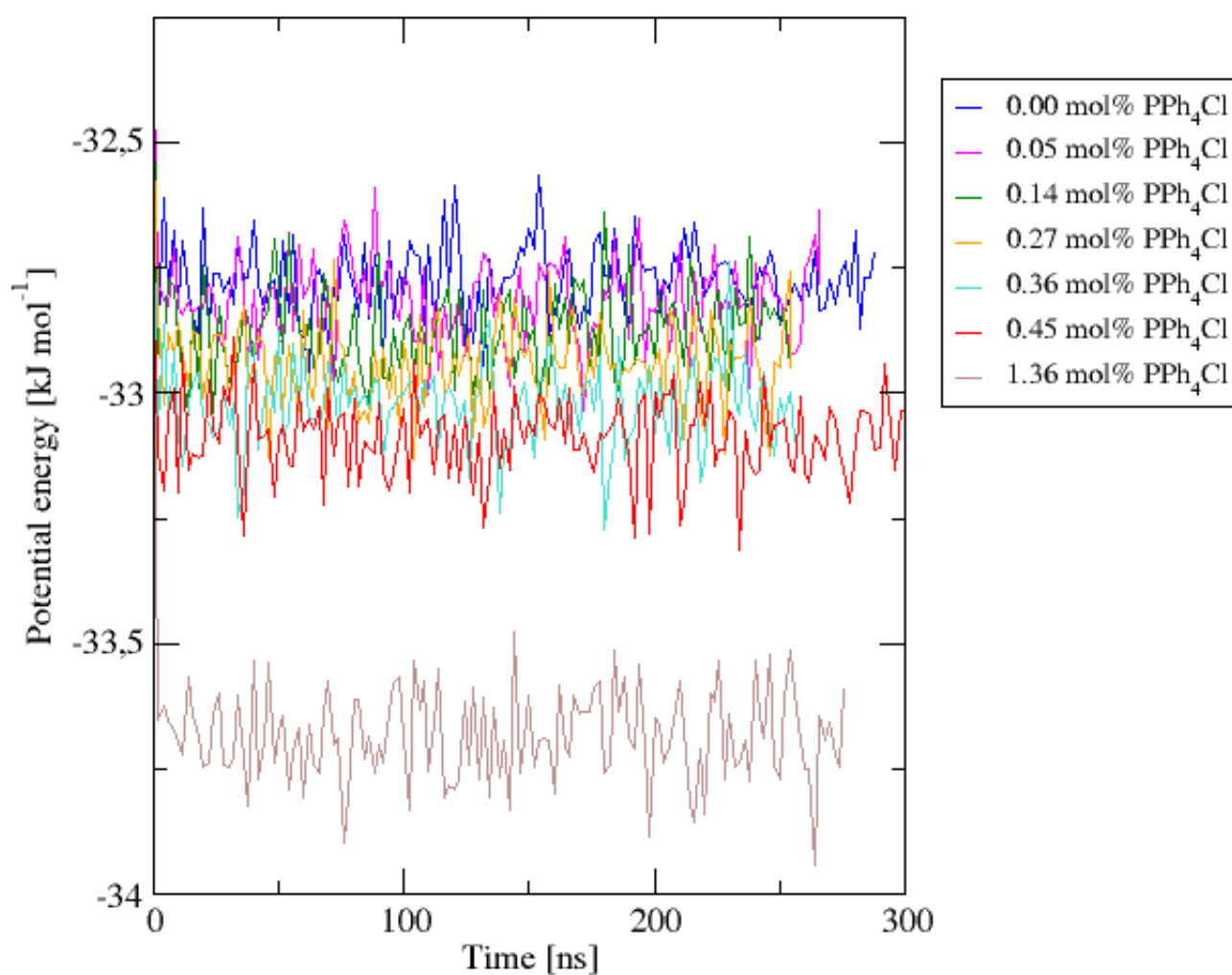


Figure 5.14: Potential energy $U(t)$ between all molecules in the system per molecule of water for all systems with different mol% of PPh₄Cl at $T_{sim} = 380$ K and $p_{sim} = 1$ bar.

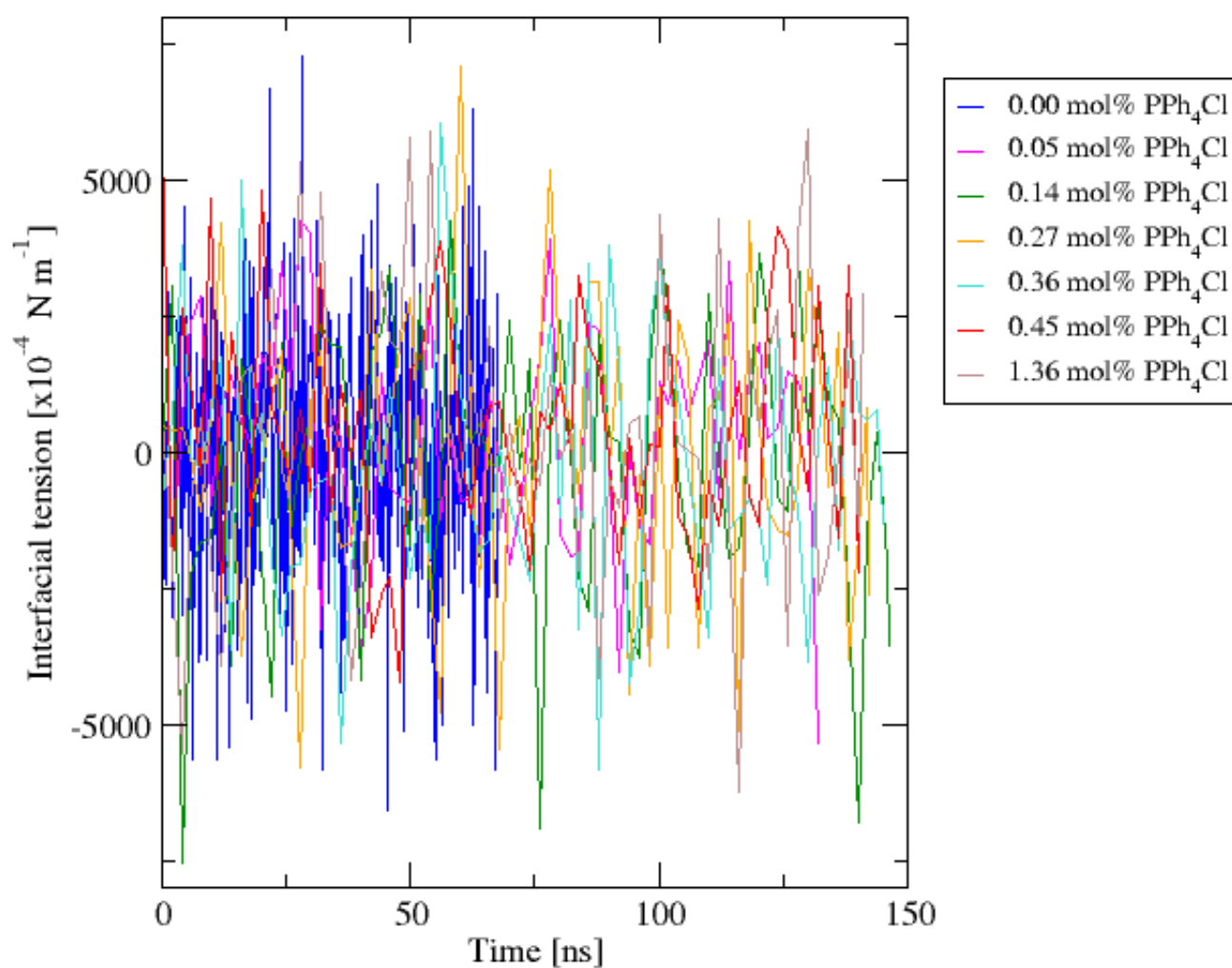


Figure 5.15: Interfacial tension $\gamma(t)$ for all systems with different mol% of PPh₄Cl at $T_{sim} = 380$ K and $p_{sim} = 1$ bar.

5.5 Simulation Results

Table 5.1 presents physical quantities for the water/2,6-lutidine systems with different concentrations of salt at equilibrium at $T_{sim} = 380$ K. The results were extracted from time frames started at 150 ns and throughout the simulation time, except interfacial tension from 25 ns to the times stated in section 5.1.

Table 5.2 presents the average number of hydrogen bonds per time frame between water and water per water molecule, and between water and 2,6-lutidine per 2,6-lutidine molecule.

Table 5.1: Simulated results for various physical quantities of the water/2,6-lutidine system with different salt concentrations after NPT at $T_{sim} = 380$ K. The symbol ρ denotes density of the whole system, T temperature, p pressure, C_p heat capacity at constant pressure, U potential energy, and γ interfacial tension. C_p and U are calculated per molecule of the system. and γ is given for the entire bilayer. All quantities were simulated with the Parrinello-Rahman barostat, except γ which was simulated with Berendsen.

mol% PPh ₄ Cl	T [K]	p [bar]	ρ [kg m ⁻³]	C_p [J mol ⁻¹ K ⁻¹]	U [kJ mol ⁻¹]	γ [·10 ⁻⁴ N m ⁻¹]
0.00	379.87 ± 0.17	1.98 ± 0.03	881.87 ± 0.24	188.01	-32.77	68.22 ± 3.5
0.05	379.98 ± 0.23	1.79 ± 0.03	883.62 ± 0.26	204.48	-32.81	54.80 ± 2.8
0.14	380.26 ± 0.21	1.57 ± 0.06	886.51 ± 0.27	216.84	-32.87	42.78 ± 3.6
0.27	380.09 ± 0.22	1.30 ± 0.06	889.85 ± 0.31	231.90	-32.94	20.14 ± 3.1
0.36	379.80 ± 0.22	1.26 ± 0.06	892.31 ± 0.33	238.01	-33.02	17.41 ± 3.4
0.45	379.68 ± 0.14	1.09 ± 0.06	895.33 ± 0.17	244.64	-33.08	5.71 ± 3.3
1.36	379.99 ± 0.23	1.02 ± 0.07	918.70 ± 0.20	293.83	-33.68	-6.40 ± 1.4

Table 5.2: Average number of hydrogen bonds between water and water per water molecule, and between water and 2,6-lutidine per 2,6-lutidine molecule.

mol% PPh ₄ Cl	Number of hydrogen bonds	
	water and water	water and 2,6-lutidine
0.00	1.415	0.646
0.05	1.413	0.643
0.14	1.406	0.648
0.27	1.392	0.667
0.36	1.383	0.686
0.45	1.372	0.708

Chapter 6

Discussion

The aim of this master's thesis is to confirm that interfacial tension decreases as concentration of antagonistic salt increases. This chapter will review a few simulation parameters and the systems will be discussed in detail.

6.1 Simulation Parameters

6.1.1 Simulation Times

As stated in section 5.1, a suitable equilibrium time was chosen for defining time frames from where Gromacs programs would calculate averaged results. As mention in step 5 in 4.2, the selected equilibrium time is important to extract the best results possible out of the already finished simulations. The quantities displayed in figure 5.12 – 5.14 and additional graphs for quantities not pictured in this thesis, were studied extensively to determine a suitable equilibrium time for the NPT simulation with the Parrinello-Rahman barostat. The equilibrium time was set to 150 ns, as it is far enough from the unstabilized initial parts of the curves, and gives the Gromacs programs good enough data to calculate good averaged results.

It can be hard to determine where the unstabilized part of a quantity curve ends, but for figure 5.1b that shows exactly this. From 0 to 10 ns, the curve is defined in the range of 800 to 885 kg m^{-3} , with the average of $867.57 \pm 13.47 \text{ kg m}^{-3}$. Between 150 and 286 ns the average is now calculated to $881.87 \pm 0.24 \text{ kg m}^{-3}$. The difference is considerable. This example shows the necessity of good preparatory studies before deciding on a simulation time, or equilibrium time, for calculations.

6.1.2 Temperature and Pressure Coupling

The results of temperature and pressure seen in table 5.1 are approximately equal to the chosen values, $T_{sim} = 380 \text{ K}$ and $p_{sim} = 1 \text{ bar}$. The curve in figure 5.1a shows the temperature during

NPT simulation corresponds to the system with 0.00 mol% salt. As seen from the graphs, the temperature fluctuates.

Temperatures are in MD simulations with Gromacs computed by the total kinetic energy of the system [35]. As the kinetic energy fluctuates, temperature follows. The goal is not to fix the temperature, but to ensure that the averaged value for temperature of the system is correct. Since the kinetic energy fluctuates, temperature does too consequently. As the simulation goes by, the average over the fluctuations will be approximately equal to T_{sim} . This is also valid for larger systems.

Pressure is calculated by both the virial and the kinetic energy [35], and will fluctuate as well. The average fluctuations will be approximately equal to p_{sim} .

6.2 Molecular Configurations and Partial Density Profiles

The total densities for the seven systems are shown in figure 5.12. As the concentrations of PPh_4Cl is increased, the total density of the system follows. This seems natural as the molar mass of PPh_4Cl is $374.85 \text{ g mol}^{-1}$ which is almost four times more than the molar mass of 2,6-lutidine. As n water molecules are replaced with n chloride anions when PPh_4Cl is added, and the molar mass of water and chloride anions are quite similar, the amount of these molecules do not influence the total density. This is the reason the total density of the systems shifts to higher densities as the concentration of PPh_4Cl increases.

This chapter will discuss the relationship between the molecular configurations and the partial density profile, as the total density has been discussed above.

6.2.1 Binary Mixture of Water and 2,6-Lutidine

Figure 5.2 shows the molecular configuration of the equilibrated water/2,6-lutidine system. The two phases and the interface in between are clearly visible in the x/y-plane. The configuration, in combination with thorough studies of the equilibrated quantities, imply that the initial system is located in the miscibility gap, as was the intention outlined in section 4.1. The presence of the interface implies that there are less hydrogen bonds between 2,6-lutidine and water in the miscibility gap than in the rest of the system.

The partial density profile for the system is shown in figure 5.9a. As the profile shows, the system has two clearly separated phases with a clear interface. The curves are fairly squared, so across the interface the concentration of water will nearly "jump" to a low concentration and 2,6-lutidine vice versa. The density profile also indicate that the two phases are water-rich and 2,6-lutidine-rich as described in section 2.3. In the water-rich phase small amounts of 2,6-lutidine exists, and in the 2,6-lutidine-rich phase small amounts of water exists.

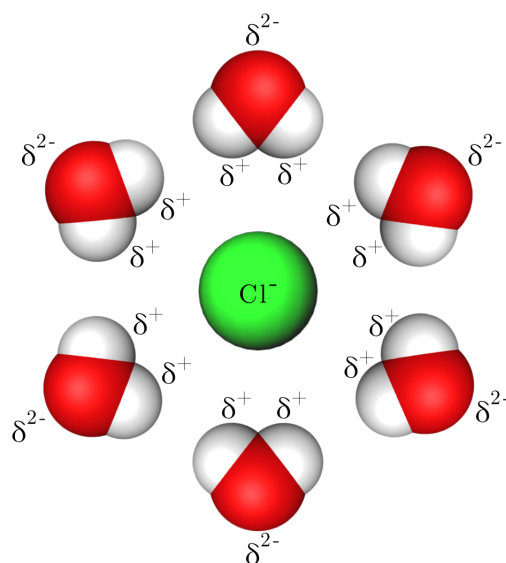


Figure 6.1: Illustration of the innermost hydration shell surrounding a chloride anion. The green atom in the middle is the chloride anion, with water molecules around. δ^+ and δ^{2-} indicates the partial charges of the water molecules.

6.2.2 Systems with Low Concentrations of PPh_4Cl

This section discusses the systems with 0.05 mol% and 0.14 mol% PPh_4Cl . The equilibrated molecular configurations are shown in figure 5.3 and 5.4, and the partial density profile for the system with 0.14 mol% PPh_4Cl in figure 5.9b.

This thesis is based on the theory that when small concentrations of antagonistic salt is added to a binary mixture of water/2,6-lutidine, the salt will distribute evenly along the interfaces. The molecular configurations shows that when 0.05 mol% and 0.14 mol% PPh_4Cl are added to the mixture, the salt evenly distributes along the interfaces after NPT. This can also be seen in figure 5.11a, with high peaks indicating the highest density of salt at the interfaces.

Figure 5.11a shows clearly that the concentration of Cl^- anions in the 2,6-lutidine-rich phase is close to zero. This can also be seen from the molecular configuration in figure 5.4. The anions in the system will be surrounded by hydration shells as described in section 2.5.1. These hydration shells makes the anions strongly hydrophilic, causing them to end up in the water-rich phase. A hydration shell consists of many layers of water molecules, and figure 6.1 illustrates the innermost shell. Hydrogen bonds surrounding larger organic molecules, as PPh_4^+ , will be deformed and the cations will acquire hydrophobicity and tend to stay at the 2,6-lutidine rich side of the interfaces.

The location of the interfaces for the 0.14 mol% PPh_4Cl system are presented in figure 5.10b, where the two density profiles intercepts. As the interfaces are distinct, it can be assumed that the mixture is unsaturated with respect to salt. Nevertheless, the density profiles in the figure is slightly more rounded than the density profiles for the figure of just water and 2,6-lutidine (figure 5.10a). This implies that the water-rich phase has become slightly less water-rich and the 2,6-lutidine-rich phase slightly less 2,6-lutidine-rich. Another way this is implied is by the higher

density of 2,6-lutidine in the water-rich phases. It is plausible that some of the previously broken hydrogen bonds, were re-formed causing the miscibility gap to be reduced in size. In addition, the density of water will decrease as the concentration of salt is increased, as water molecules are replaced with chloride anions.

6.2.3 Systems with Medium Concentrations of PPh_4Cl

This section discusses the systems with 0.27 mol%, 0.36 mol%, and 0.45 mol% PPh_4Cl . The equilibrated molecular configurations are shown in figure 5.5 – 5.7, and the partial density profile for the system with 0.36 mol% PPh_4Cl in figure 5.9c.

The interfaces in these three systems are more undefined than in systems with lower concentrations of salt. A smoother transition between water and 2,6-lutidine can be seen in the respectively molecular configurations, as well as in figure 5.10c. The partial density profile is more rounded compared to systems with lower concentrations of salt. This is probably a sign of decreasing interfacial tension as the concentration of PPh_4Cl increases. Even though the transition is fairly smooth, the system will still consist of two separate phases and a miscibility gap will be present.

It seems like the distribution of PPh_4Cl in the water-rich phases in the molecular configurations, is now not only at the interface. This is especially clear in figure 5.7. The observation is further substantiated by the density curves of the salt shown in figure 5.11b. Where there were peaks in systems with lower concentrations, there is now "edges". The change of salt density in the 2,6-lutidine-rich phase is steep, but in the water-rich phases the curves evens out. This is assumed to imply that the former hydrophobic cations are now less hydrophobic, because of the small formation of hydration shells surrounding the cations in addition to anions. As the water now needs to form hydration shells surrounding the cations as well as the anions, the amount of water may not be enough to form good enough hydration shells for the growing amount of chloride anions. The concentration of salt could even be so high the interface area is not big enough to accommodate the salt molecules that wants to adsorb close to the interface.

The smoother transition between water and 2,6-lutidine leads to higher amounts of water molecules in the oil-rich phase, and 2,6-lutidine in the water-rich phase. This suggests that an increasing number of hydrogen bonds between 2,6-lutidine and water are formed as the concentration of salt increases. As there will be more 2,6-lutidine in the water-rich phase, more cations will also be present in this phase. This is probably not the case for the amount of anions in the 2,6-lutidine phase, as the molecular configurations and density profiles implies. There is probably enough water in the system to form hydration shells surrounding parts of the chloride anions.

This section further indicates that the interfacial tension of the binary water/2,6-lutidine mixture decreases when antagonistic salts are added.

6.2.4 Systems with High Concentrations of PPh_4Cl

This section discusses the system with 1.36 mol% PPh_4Cl . The equilibrated molecular configuration is shown in figure 5.8, and the partial density profile for the system in figure 5.9d.

The molecular configuration and the density profile shows a homogeneous system with cations and anions evenly distributed throughout the whole system. This is even clearer in the partial density profiles for water and 2,6-lutidine in figure 5.10d, as well as the profile for cations and anions in figure 5.11c.

The density profile of the mixture do not show any phase boundaries. The two-phased miscibility gap that was assumed to exist for systems with lower and medium concentrations of salt is considered to be non-existent. As this is considered to be a homogeneous system, interfaces will be non-existent. Interfacial tension will also be non-existent, or even negative as Onuki and Araki implies [43]. Hydrogen bonds between water and 2,6-lutidine are probably established as in the homogeneous phase described in section 2.3.

The hydration shells that are formed around chloride anions at lower and medium salt concentrations are in this system probably non-existent. The concentration of salt is so high that it is not enough water to form hydration shells. The number of hydrogen bonds between 2,6-lutidine and water increases compared to systems with lower salt concentrations, and the number of hydrogen bonds in between water molecules decreases. It almost seems like this system behaves more like an ionic liquid at this temperature.

6.3 Hydrogen Bonds

As the previous sections assumes, the number of hydrogen bonds between 2,6-lutidine and water increase by increasing salt concentrations. This is confirmed by the results shown in table 5.2 and curves in figure 5.13. The table also shows that the number of hydrogen bonds in between water molecules in the systems decrease as the concentration of salt increases, which is also assumed in the previous sections.

The phase separation and presence of a homogeneous phase in the binary mixture, can be explained by formations and deformations of hydrogen bonds, as described in section 2.3.

6.4 Intermolecular Potential Energy

The results of the calculations of average intermolecular potential energies are stated in table 5.1, and the fluctuating curves are seen in figure 5.14. The energies are negative. This implies that there is a large portion of attractive forces in the liquid systems. As the salt concentration increases, the potential energies of the systems are shifted to even lower values. This is assumed to imply that the systems with higher salt concentrations have more attractive forces and that the systems are at a higher bound state.

Potential energies between molecules in a liquid will fluctuate, but as seen by the curves in figure 5.14, they fluctuate around an average value. As potential energy is one of the basis of MD simulations, it is really important that these values are equilibrated sufficiently, which is assumed accomplished.

6.5 Molar Heat Capacity at Constant Pressure

For the systems with higher salt concentrations, the molar heat capacity will at constant pressure be higher than for systems with lower concentrations, as assumed. Table 5.1 shows this per molecule of the system.

6.6 Interfacial Tension

The results of the calculations of average interfacial tensions with the Berendsen barostat are stated in table 5.1, and the fluctuating curves are seen in figure 5.15. These results seem to support the aim of this thesis, which was to confirm that additions of antagonistic salts to the binary water/2,6-lutidine mixture will decrease the systems interfacial tension. The values of interfacial tension in table 5.1 decrease from 54.8 to $7.71 \cdot 10^{-4} \text{ N mol}^{-1}$ for the systems with miscibility gaps, and further decreased to $-6.4 \cdot 10^{-4} \text{ N mol}^{-1}$ for what seems to be a homogeneous system.

6.7 Sources of Error

The results in table 5.2 show a high number of hydrogen bonds between water and 2,6-lutidine per 2,6-lutidine molecule, compared to the systems with antagonistic salt. It was assumed the number of hydrogen bonds between water and 2,6-lutidine per 2,6-lutidine molecule in the system with 0.00 mol% PPh_4Cl would be slightly lower than the system with 0.05 mol% PPh_4Cl . The assumption was grounded in two well separated phases in the water/2,6-lutidine system. The partial density profile for the water/2,6-lutidine system shows in figure 5.10a, that there are small amounts of 2,6-lutidine in the water-rich phase, as previously mentioned. This could be the reason for the high number of hydrogen bonds between water and 2,6-lutidine per 2,6-lutidine molecule.

There might be some errors in the simulations, calculations of the hydrogen bonds between water and 2,6-lutidine per 2,6-lutidine molecule, or in the equilibrations of the systems. It was assumed the simulations, calculations, and equilibrations were completed in a satisfying manner, but there is possibly a source of error somewhere in the process. If we can identify the potential error, correct it, and replicate the simulations, the results can be further verified.

The partial density profiles were computed over a fairly long period of time. It is assumed the profiles would have been even smoother in appearance if the profiles were computed in a shorter time span, at e.g. 200 ns to 250 ns. Even clearer results could give clearer graphs.

Chapter 7

Conclusion

The aim of this master's thesis has been to confirm that the interfacial tension in a binary mixture will be reduced as antagonistic salt is introduced. The binary mixture consists of water, the organic solvent 2,6-lutidine, and the chosen antagonistic salt PPh_4Cl . The interfacial tension was expected to decrease as the concentration of antagonistic salt was increased. The study was completed by means of MD simulations.

To study the effect, seven systems were produced with salt concentrations ranging from 0.00 mol% to 1.36 mol% PPh_4Cl . To construct the systems the TIP4P/2005 model was chosen for water, and the 2,6-lutidine model and PPh_4Cl model proposed by Pousaneh et al. for 2,6-lutidine and salt. The simulations were simulated with the GROMOS 45A7 force field by the MD package Gromacs, and the supercomputer Vilje was used to reduce the time used for simulating the systems.

From the equilibrated systems produced by the NPT ensemble, results were extracted and presented as molecular configurations and quantitative results. The results shown in chapter 5 clearly shows that the interfacial tension of the binary water/2,6-lutidine mixture decreases as the concentration of the antagonistic salt PPh_4Cl increases. For the systems with 0.00 mol% to 0.45 mol% PPh_4Cl a decrease in interfacial tension can be seen by both the molecular configurations and the quantitative results. For the system with 1.36 mol% PPh_4Cl the two-phased coexistence loop could not be confirmed, so it is assumed that the miscibility gap for this system is non-existent, which causes no interfaces to be present. The interfacial tension for this system was found to be negative.

Some minor potential errors have been discussed. Even if these errors prove to be real, they are assumed to be sufficiently insignificant, making the theory and conclusion of this thesis valid.

Chapter 8

Further Work

As observed in this master's thesis, the concentration of the antagonistic salt plays an important part in the interfacial tension in a binary water/oil system. Different concentrations of salt has been introduced, and it is plausible that the miscibility gap ceases to exist somewhere between the concentrations 0.45 mol% and 1.36 mol% PPh₄Cl. Further work can include discovering at what exact concentration of antagonistic salt the system will completely mix and the miscibility gap disappears. Other approaches could be to study how these salts can effect viscosity and friction in water/oil systems.

In addition an effort could be made to replicate these simulations. This could both further validate the results in this thesis, as well as possibly find the potential source of error.

References

- [1] Jose LF Abascal and Carlos Vega. A general purpose model for the condensed phases of water: Tip4p/2005. *The Journal of chemical physics*, 123(23):234505, 2005.
- [2] Mark James Abraham, Teemu Murtola, Roland Schulz, Szilárd Páll, Jeremy C Smith, Berk Hess, and Erik Lindahl. Gromacs: High performance molecular simulations through multi-level parallelism from laptops to supercomputers. *SoftwareX*, 1:19–25, 2015.
- [3] Michael P Allen et al. Introduction to molecular dynamics simulation. *Computational soft matter: from synthetic polymers to proteins*, 23:1–28, 2004.
- [4] Hans C Andersen. Molecular dynamics simulations at constant pressure and/or temperature. *The Journal of chemical physics*, 72(4):2384–2393, 1980.
- [5] Yael Avissar, Jung Choi, and Jean DeSaix. *Biology*. OpenStax College, 2013. ISBN 9781938168093.
- [6] Herman JC Berendsen, JPM van Postma, Wilfred F van Gunsteren, ARHJ DiNola, and JR Haak. Molecular dynamics with coupling to an external bath. *The Journal of chemical physics*, 81(8):3684–3690, 1984.
- [7] Giovanni Bussi, Davide Donadio, and Michele Parrinello. Canonical sampling through velocity rescaling. *The Journal of chemical physics*, 126(1):014101, 2007.
- [8] John Hughes (contributor) Raymond A Serway Chris Vuille. *College Physics, Global Edition*. CENGAGE Learning Custom Publishing, oct 2017. ISBN 1337620335.
- [9] MM Conde, MA Gonzalez, JLF Abascal, and C Vega. Determining the phase diagram of water from direct coexistence simulations: The phase diagram of the tip4p/2005 model revisited. *The Journal of chemical physics*, 139(15):154505, 2013.
- [10] Tom Darden, Darrin York, and Lee Pedersen. Particle mesh ewald: An $n \log(n)$ method for ewald sums in large systems. *The Journal of chemical physics*, 98(12):10089–10092, 1993.
- [11] Gromacs development team. *Gromacs: Command-line reference*. URL <http://manual.gromacs.org/documentation/2018/user-guide/cmdline.html>. Accessed: 2019-06-16.
- [12] D Joseph Donahue and FE Bartell. The boundary tension at water-organic liquid interfaces. *The Journal of Physical Chemistry*, 56(4):480–484, 1952.
- [13] Ulrich Essmann, Lalith Perera, Max L Berkowitz, Tom Darden, Hsing Lee, and Lee G Pedersen. A smooth particle mesh ewald method. *The Journal of chemical physics*, 103(19): 8577–8593, 1995.

- [14] Andrea Gambassi, Anna Maciołek, Christopher Hertlein, Ursula Nellen, Laurent Helden, Clemens Bechinger, and Siegfried Dietrich. Critical casimir effect in classical binary liquid mixtures. *Physical Review E*, 80(6):061143, 2009.
- [15] Miguel A González and José LF Abascal. A flexible model for water based on tip4p/2005. *The Journal of chemical physics*, 135(22):224516, 2011.
- [16] David Jeffery Griffiths. *Introduction to Quantum Mechanics*. Pearson Prentice Hall, 2005. ISBN 0131118927. Chapter 1.
- [17] Marcus D Hanwell, Donald E Curtis, David C Lonie, Tim Vandermeersch, Eva Zurek, and Geoffrey R Hutchison. Avogadro: an advanced semantic chemical editor, visualization, and analysis platform. *Journal of cheminformatics*, 4(1):17, 2012.
- [18] J. B. Hasted. *Liquid water: Dielectric properties, in Water A comprehensive treatise*. Plenum Press, 1972.
- [19] Wolfgang. Horsch Martin. Bungartz Hans-Joachim Heinecke, Alexander. Eckhardt. *Supercomputing for Molecular Dynamics Simulations*. Springer, SpringerBriefs in Computer Science, 2015.
- [20] Berk Hess, Henk Bekker, Herman JC Berendsen, and Johannes GEM Fraaije. Lincs: a linear constraint solver for molecular simulations. *Journal of computational chemistry*, 18(12):1463–1472, 1997.
- [21] William Humphrey, Andrew Dalke, and Klaus Schulten. VMD – Visual Molecular Dynamics. *Journal of Molecular Graphics*, 14:33–38, 1996.
- [22] Jong Cheol Jo and Byeong Cheol Kim. Determination of proper time step for molecular dynamics simulation. *Bulletin of the Korean Chemical Society*, 21(4):419–424, 2000.
- [23] George Kaptay. On the negative surface tension of solutions and on spontaneous emulsification. *Langmuir*, 33(40):10550–10560, 2017.
- [24] Naoki Karasawa and William A Goddard III. Acceleration of convergence for lattice sums. *The Journal of Physical Chemistry*, 93(21):7320–7327, 1989.
- [25] V Kumaran. Josiah willard gibbs. *Resonance*, 12(7):4–11, 2007.
- [26] Mostafa Lashkarbolooki, Shahab Ayatollahi, and Masoud Riazi. Mechanistic study on the dynamic interfacial tension of crude oil+ water systems: Experimental and modeling approaches. *Journal of industrial and engineering chemistry*, 35:408–416, 2016.
- [27] B. Lautrup. *Physics of Continuous Matter: Exotic and Everyday Phenomena in the Macroscopic World*, volume Chapter 5. CRC Press, dec 2004. ISBN 0750307528.
- [28] Justin A. Lemkul. Gromacs tutorial: Lysozyme in water. <http://www.mdtutorials.com/gmx/lysozyme/index.html>, Accessed: 2019-06-16.
- [29] Irene Ly Libretexs Cameron Tracy, Ling Xie. Cohesive and adhesive forces, June 5th 2019. URL [https://chem.libretexs.org/Bookshelves/Physical_and_Theoretical_Chemistry_Textbook_Maps/Supplemental_Modules_\(Physical_and_Theoretical_](https://chem.libretexs.org/Bookshelves/Physical_and_Theoretical_Chemistry_Textbook_Maps/Supplemental_Modules_(Physical_and_Theoretical_)

- Chemistry)/Physical_Properties_of_Matter/States_of_Matter/Properties_of_Liquids/Cohesive_and_Adhesive_Forces. Accessed: 2019-06-12.
- [30] Guangming Luo, Sarka Malkova, Jaesung Yoon, David G Schultz, Binhua Lin, Mati Meron, Ilan Benjamin, Petr Vanýsek, and Mark L Schlossman. Ion distributions near a liquid-liquid interface. *Science*, 311(5758):216–218, 2006.
- [31] J. Lyklema. *Fundamentals of Interface and Colloid Science: Liquid-Fluid Interfaces*, volume III, chapter 1–2. Academic Press, 2000. ISBN 0124605230.
- [32] Julien Marcus. *Study of surfactant-free microemulsions and microemulsions with fatty acid salts*. PhD thesis, Institute of Physical and Theoretical Chemistry, University of Regensburg, 2015.
- [33] Aleksandar Mehandzhiyski. Lecture notes of md simulations with gromacs, April 2016. URL http://www.virtualsimlab.com/s/VSL_GROMACS-6tt5.pdf, Accessed: 2019-06-26, Virtual Simulation Lab, Faculty of Natural Sciences and Technology, Norwegian University of Science and Technology.
- [34] Dominik Michler, Noushine Shahidzadeh, Marise Westbroek, Rene van Roij, and Daniel Bonn. Are antagonistic salts surfactants? *Langmuir*, 31(3):906–911, 2015.
- [35] E. Lindahl-B. Hess M.J. Abraham, D. van der Spoel and the Gromacs development team. *Gromacs User Manual 2018*, www.gromacs.org (2018), 2018.
- [36] T Narayanan and Anil Kumar. Reentrant phase transitions in multicomponent liquid mixtures. *Physics Reports*, 249(3):135–218, 1994.
- [37] National Center for Biotechnology Information. 2,6-lutidine, 2018. PubChem Compound Database, <https://pubchem.ncbi.nlm.nih.gov/compound/7937>, Accessed: 2018-12-11.
- [38] National Center for Biotechnology Information. Water, 2018. PubChem Compound Database, <https://pubchem.ncbi.nlm.nih.gov/compound/Water>, Accessed: 2018-12-11.
- [39] National Center for Biotechnology Information. Tetraphenylphosphonium chloride, 2019. PubChem Compound Database, <https://pubchem.ncbi.nlm.nih.gov/compound/Tetraphenylphosphonium-chloride>, Accessed: 2019-07-05.
- [40] Erik C Neyts and Annemie Bogaerts. Combining molecular dynamics with monte carlo simulations: implementations and applications. In *Theoretical Chemistry in Belgium*, pages 277–288. Springer, 2014.
- [41] Koji Nishida, Hideyuki Morita, Yutaka Katayama, Rintaro Inoue, Toshiji Kanaya, Koichiro Sadakane, and Hideki Seto. Salting-out and salting-in effects of amphiphilic salt on cloud point of aqueous methylcellulose. *Process Biochemistry*, 59:52–57, 2017.
- [42] Akira Onuki. Ginzburg-landau theory of solvation in polar fluids: Ion distribution around an interface. *Physical Review E*, 73(2):021506, 2006.
- [43] Akira Onuki and Takeaki Araki. Selective solvation in aqueous mixtures: interface deformations and instability. *Journal of the Physical Society of Japan*, 81(Suppl. A):SA004, 2012.

- [44] Akira Onuki, Shunsuke Yabunaka, Takeaki Araki, and Ryuichi Okamoto. Structure formation due to antagonistic salts. *Current Opinion in Colloid & Interface Science*, 22:59–64, 2016.
- [45] Libretexts Jose Pietri. Hydrogen bonding, June 5th 2019. URL [https://chem.libretexts.org/Bookshelves/Physical_and_Theoretical_Chemistry_Textbook_Maps/Supplemental_Modules_\(Physical_and_Theoretical_Chemistry\)/Physical_Properties_of_Matter/Atomic_and_Molecular_Properties/Intermolecular_Forces/Specific_Interactions/Hydrogen_Bonding](https://chem.libretexts.org/Bookshelves/Physical_and_Theoretical_Chemistry_Textbook_Maps/Supplemental_Modules_(Physical_and_Theoretical_Chemistry)/Physical_Properties_of_Matter/Atomic_and_Molecular_Properties/Intermolecular_Forces/Specific_Interactions/Hydrogen_Bonding). Accessed: 2019-06-26.
- [46] David Dowling Pijush K. Kundu, Ira Cohen. *Fluid mechanics*. Academic Press, 5th edition, 2012. ISBN 0-12-382101-0.
- [47] Faezeh Pousaneh, Olle Edholm, and Anna Maciołek. Molecular dynamics simulation of a binary mixture near the lower critical point. *The Journal of chemical physics*, 145(1):014501, 2016.
- [48] Peter H Raven, George B Johnson Professor, Kenneth A. Mason Dr. Ph.D., Jonathan Losos Dr., and Susan Singer. *Biology*. McGraw-Hill Education, 2016. ISBN 1259188132.
- [49] Koichiro Sadakane and Hideki Seto. Membrane formation in liquids by adding an antagonistic salt. *Frontiers in Physics*, 6:26, 2018.
- [50] Koichiro Sadakane, Akira Onuki, Koji Nishida, Satoshi Koizumi, and Hideki Seto. Multilamellar structures induced by hydrophilic and hydrophobic ions added to a binary mixture of d₂o and 3-methylpyridine. *Physical review letters*, 103(16):167803, 2009.
- [51] Koichiro Sadakane, Natsuki Iguchi, Michihiro Nagao, Hitoshi Endo, Yuri B Melnichenko, and Hideki Seto. 2d-ising-like critical behavior in mixtures of water and 3-methylpyridine including antagonistic salt or ionic surfactant. *Soft Matter*, 7(4):1334–1340, 2011.
- [52] Koichiro Sadakane, Yuka Horikawa, Michihiro Nagao, and Hideki Seto. The effect of tetraphenylphosphonium chloride on phase behavior and nanoscale structures in a mixture of d₂o and 3-methylpyridine. *Chemistry Letters*, 41(10):1075–1077, 2012.
- [53] Koichiro Sadakane, Michihiro Nagao, Hitoshi Endo, and Hideki Seto. Membrane formation by preferential solvation of ions in mixture of water, 3-methylpyridine, and sodium tetraphenylborate. *The Journal of chemical physics*, 139(23):234905, 2013.
- [54] Koichiro Sadakane, Hitoshi Endo, Koji Nishida, and Hideki Seto. Lamellar/disorder phase transition in a mixture of water/2, 6-dimethylpyridine/antagonistic salt. *Journal of Solution Chemistry*, 43(9-10):1722–1731, 2014.
- [55] Nathan Schmid, Andreas P Eichenberger, Alexandra Choutko, Sereina Riniker, Moritz Winger, Alan E Mark, and Wilfred F van Gunsteren. Definition and testing of the gromos force-field versions 54a7 and 54b7. *European biophysics journal*, 40(7):843, 2011.
- [56] Toshiaki Kataoka Takayuki Shoji-Nobuyuki Abe Sinji Morishita Shinkichi Shimizu, Nanao Watanabe and Hisao Ichimura. Pyridine and pyridine derivatives. *Ullmann's Encyclopedia of Industrial Chemistry*, 2000.

- [57] Barry R Silver, Karel Holub, and Vladimir Mareček. Spontaneous emulsification at surfactantless liquid/liquid interfaces. *Journal of Electroanalytical Chemistry*, 805:91–97, 2017.
- [58] Pier Luigi Silvestrelli and Michele Parrinello. Structural, electronic, and bonding properties of liquid water from first principles. *The Journal of chemical physics*, 111(8):3572–3580, 1999.
- [59] Toshiyuki Takamuku, Atsushi Yamaguchi, Daisuke Matsuo, Masaaki Tabata, Midori Kumamoto, Jun Nishimoto, Koji Yoshida, Toshio Yamaguchi, Michihiro Nagao, Toshiya Otomo, et al. Large-angle x-ray scattering and small-angle neutron scattering study on phase separation of acetonitrile- water mixtures by addition of nacl. *The Journal of Physical Chemistry B*, 105(26):6236–6245, 2001.
- [60] Sigma 2 Uninett. Vilje ntnu hpc group. URL <https://www.hpc.ntnu.no/display/hpc/Vilje>. Accessed: 2019-06-03.
- [61] David Van Der Spoel, Erik Lindahl, Berk Hess, Gerrit Groenhof, Alan E Mark, and Herman JC Berendsen. Gromacs: fast, flexible, and free. *Journal of computational chemistry*, 26(16):1701–1718, 2005.
- [62] Wilfred F van Gunsteren and Herman JC Berendsen. Computer simulation of molecular dynamics: Methodology, applications, and perspectives in chemistry. *Angewandte Chemie International Edition in English*, 29(9):992–1023, 1990.
- [63] Carlos Vega and Jose LF Abascal. Simulating water with rigid non-polarizable models: a general perspective. *Physical Chemistry Chemical Physics*, 13(44):19663–19688, 2011.
- [64] Edward Vigmond. *Grace User's Guide (Grace-5.1.4)*. <http://plasma-gate.weizmann.ac.il/Grace/doc/Tutorial.html#toc2>, Accessed: 2019-06-26.
- [65] Robert Winkler, Thomas Buchecker, Florian Hastreiter, Didier Touraud, and Werner Kunz. Pph 4 cl in aqueous solution—the aggregation behavior of an antagonistic salt. *Physical Chemistry Chemical Physics*, 19(37):25463–25470, 2017.
- [66] Monika Witala, Sebastian Lages, and Kim Nygård. Mesoscale ordering in binary aqueous solvents induced by ion size asymmetry. *Soft matter*, 12(21):4778–4782, 2016.

Appendix A

Basics of Gromacs

This appendix is an excerpt from the pre-master's thesis finished January 7th, 2019 by the author of this master's thesis, Gudrun Glende.

This appendix is mainly based on the Gromacs reference manual written by M.J. Abraham and the Gromacs development team. For further reading and more details, see the Gromacs user manual, reference [35].

A.1 Periodic Boundary Conditions

For MD in general, a system is often referred to as a box with finite size. With finite sizes edges will be present. Edges will interact with particles in the system and influence the movement of the particles, as the particles "crashes" into the edges. This is an undesired effect in MD simulations. The general way to decrease this effect, is to introduce *periodic boundary conditions* for the Gromacs simulation. The system is surrounded by replicas of itself as shown in figure A.1. If a real particle moves out of the real system, an image particle, with the same properties, moves into the real system and replaces it. A particle in the system will then interact with both real and image particles, as shown by the dashed line in the figure. This way of simulating interactions in the periodic array is described as *minimum image convention* [3].

The minimum image convention states that the cut-off radius for non-bonded interactions may not be longer than half of the shortest box vector. If the cut-off radius is longer than this, there will be more than one image particle to take into account. More about molecular interactions in section A.2.

For long-range electrostatic interactions, these conditions are not sufficient. Gromacs has therefore introduced lattice sum methods like Ewald sum and Particle-mesh Ewald (PME) for long-range electrostatic interactions. More about this in section A.4.

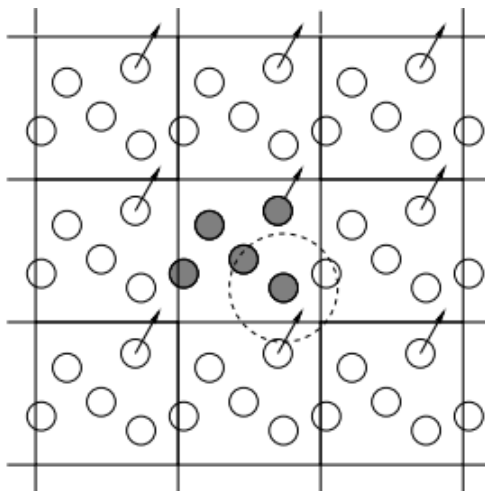


Figure A.1: Periodic boundary conditions: The original system (dark particles) surrounded by replicas [3].

A.2 Molecular Interactions

Intermolecular (non-bonded) and intramolecular (bonded) interactions are accounted for by the potential energy function V . These two interaction types contribute, with their different phenomena, to the potential energy function V :

$$V = V_{non-bonded} + V_{bonded} \quad (\text{A.1})$$

A.2.1 Non-bonded Interactions

In Gromacs, non-bonded interactions are assumed to be pair-additive. The result of this assumption is that 3-body interactions and interactions of higher order are neglected. This gives us only non-bonded interactions between two particles to consider for the non-bonded contribution to the potential energy function, given by equation (A.2) [3].

$$V_{non-bonded} = \sum_{i < j} V_{ij}(r_{ij}) \quad (\text{A.2})$$

These interactions will be centro-symmetric, as the potential will only depend on the scalar distance.

Non-bonded interactions contains three terms. A repulsion and a dispersion term, which can be described by the *Lennard-Jones interaction* or the *Buckingham potential*. And, as the third term, a *Coulomb* term which charged atoms acts through. A neighbour list where exclusions are removed, is the basis for the computation of non-bonded interactions.

Coulomb interactions is added when electrostatic charges are present. The contribution to the potential energy function by the Coulomb interaction is given by equation (A.3).

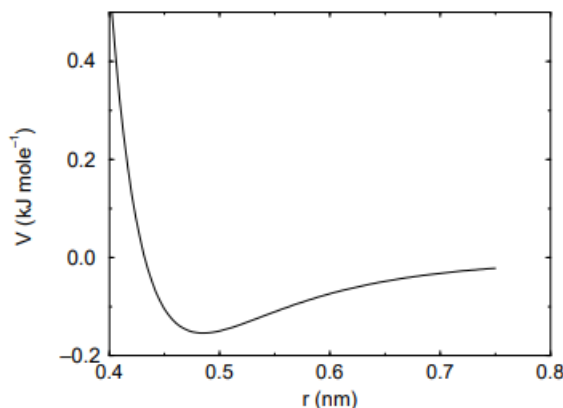


Figure A.2: The Lennard Jones interaction [35].

$$V_c(r_{ij}) = f \frac{q_i q_j}{\epsilon_r r_{ij}} \quad \text{where} \quad f = \frac{1}{4\pi\epsilon_0} \quad (\text{A.3})$$

Where f is the electric conversion factor, q_i and q_j are the partial charges of atom i and j , ϵ_r is the dielectric constant, and ϵ_0 is the permittivity of free space [3].

The **Lennard-Jones potential** describes 1) Van der Waals interactions which is present at intermediate distances, and 2) repulsion. For long range Van der Waals interactions, Gromacs assumes that the distance is long enough to neglect the repulsion term. The Lennard-Jones potential between two atoms $V_{LJ}(r_{ij})$ can be stated as equation (A.4).

$$V_{LJ}(r_{ij}) = 4\epsilon_{ij} \left[\left(\frac{\sigma_{ij}}{r_{ij}} \right)^{12} - \left(\frac{\sigma_{ij}}{r_{ij}} \right)^6 \right] \quad (\text{A.4})$$

Where ϵ_{ij} is the depth of the potential energy curve given in figure A.2 and σ_{ij} depends on the atom type and can be found in a Lennard-Jones parameters list. σ_{ij} shifts the curve described to smaller or larger values of r .

A repulsion term described by the **Buckingham potential** is more flexible and realistic than the one described by the Lennard-Jones interaction. On the other hand the Buckingham potential is more expensive to compute [35].

A.2.2 Bonded Interactions

Intramolecular interactions are interactions between atoms in molecules, which makes the movement of atoms not independent. For bonded interactions there are bond stretching (2-body), bond angles (3-body), and dihedral or torsion angles (4-body). Rotation around multiple bonds is physically not possible, and is prevented in MD simulations, by introducing *improper dihedrals*. Improper dihedrals are used to force atoms to stay in one plane throughout the simulation [3].

The contribution from bonded interactions V_{bonded} , is a sum of all the contributions from the different interactions, i.e. contributions from bond stretching, bond angles and dihedral angles [3].

A.3 Force Fields

A general force field consist of [3]:

1. a set of functional terms (Lennard-Jones, Coulomb, etc.)
2. model parameters used in these terms ($\sigma, \epsilon, etc.$)

Force fields needs to describe the interactions in a system with sufficient accuracy, so that the reproduction of properties and mechanisms represents the interactions faithfully. In Gromacs there is a number of different sets of force fields, like GROMOS, OPLS (e.g. OPLS-AA), and CHARMM [55].

Force fields can be devided into three types:

1. An **all atom** where all parameters are given for every single atom in the system (e.g. OPLS-AA).
2. An **united atom** where parameters are given for all atoms other than non-polar hydrogens (e.g. Gromacs).
3. A **coarse grained** which is an abstract way of representing several atoms as a molecule.

A.4 Electrostatics

Ewald sum and Particle-mesh Ewald (PME) are methods to compute long-range electrostatic interactions. Gromacs recommends the use of PME for all system, except very small systems where Ewald sum might be better. With PME the direct summation of interactions, done by Ewald summation, is extended to the sum of two absolutely convergent series: a direct sum in Cartesian space and a reciprocal sum in Fourier space. As a result, PME enhances the performance of the reciprocal sum [10, 13].

Compared to Ewald sum (of order $N^{3/2}$, where N is the number of atoms in the system), PME (of order $N \log(N)$) is faster on medium to larger systems [10, 24].

A.5 Statistical Ensembles

Under reproduction of experimental data, it is important to make the environment for the modelled system as equal as possible to the experimental environment. Often the system needs to have constant temperature and/or pressure. Regulation of properties like these can be done through different ensembles with use of different algorithms. An ensemble is a collection of many

indistinguishable replicas of the system studied where the replicas only interact with each other. The macroscopic state of the replicas is equal but the microscopic state can differ. The concept of ensembles were introduced by J.W. Gibbs in 1901 and is still used for computer simulations of thermodynamic properties among other things [25].

Through ensembles, like canonical (NVT) and isothermal-isobaric (NpT), temperature T and the number of particles N is constant. In addition volume V and pressure p is, respectively, also constant. Energy can for both ensembles be exchanged with the surroundings [4, 33].

A.6 Coupling Algorithms

When coupling of temperature and pressure is used, the total energy is not conserved. The total energy depends on which algorithms are used for temperature and pressure coupling and the combination of these algorithms. The grade of conservation of energy depends on the accuracy of the algorithms. Therefore it is important to use the right algorithms for MD simulations.

A.6.1 Temperature Coupling

In Gromacs there are a few different possibilities of algorithms for temperature coupling, like Berendsen weak-coupling scheme and velocity-rescaling scheme. Temperature in MD simulations is computed from the system's total kinetic energy. The goal for a thermostat is not to set the temperature to a constant value, but to ensure that the average temperature of the system is correct.

Berendsen temperature coupling is an algorithm which simulates weak coupling to an external heat bath. The fallout of Berendsen temperature coupling is a deviation of the temperature T in the system from the given temperature T_0 of the heat bath. The deviation will decrease exponentially with a time constant τ . The deviation is corrected by equation A.5 [6]:

$$\frac{dT}{dt} = \frac{T_0 - T}{\tau} \quad (\text{A.5})$$

The sampling for Berendsen temperature coupling is inaccurate since the thermostat does not take kinetic energy into consideration, so an error of $1/N$ will be present. There will therefore not be generated a correct canonical ensemble by this thermostat.

With **Velocity-rescaling temperature coupling** a proper sampling for the canonical ensemble will be generated. This thermostat is an extension of the Berendsen thermostat. The addition to Berendsen is a stochastic term that enforces the proper kinetic energy distribution [7].

A.6.2 Pressure Coupling

As for temperature coupling, there is different algorithms for pressure coupling. Two of them are Berendsen pressure coupling and Parinello-Rahm pressure coupling.

Berendsen pressure coupling changes the coordinates and box vectors with a scaling matrix for every time step. **Parinello-Rahman** changes both the size and volume of the box at every time step to control the pressure. If the pressure of the system is far from equilibrium it is expedient to first equilibrate the system to reach the targeted pressure with the weak-coupling scheme, and then use Parinello-Rahman pressure coupling for further simulations. This way the system will not be too large and the possibility for the simulation to crash is strongly reduced [6].

Both barostats can be used in combination with both Berendsen and Velocity-rescaling temperature coupling.

A.7 Constraint Algorithms

Constraints are introduced in Gromacs by either LINCS or SHAKE. LINCS is the default configuration and is used in this project, and will therefore be reviewed further.

LINCS is a linear constraint solver for MD simulations with bond constraints and isolated angle constraints. The bond vibrations is replaced with holonomic constraints after unconstrained updates, which results in the possibility for larger time steps. The LINCS algorithm is parted in two. The first part of the algorithms projects out forces working along the bonds, where the final part corrects for rotational lengthening [20].

A.8 Central Gromacs Diles

To run a Gromacs simulation three types of files are needed; topology, structure, and parameter files. These files can be either build by the user itself or found online in larger databases [17].

Topology Files

The topology file (*.top), or system topology file, contains lists of constant properties for every atom used in the system. The file contains information on which parameters that needs to be applied for different functions. It also contains information about which atoms, or mix of these, that contributes to the potential energy functions. The molecule topology file (*.itp) gives information about how the atoms are connected in a molecule, and is included in the system topology file. The force field used for the simulation is also included in the topology file [33].

Structure Files

The structure file (*.gro), or coordinate or geometry file, is an overview for the positions and velocities of the atoms in the system. In addition, the file contains the total number of atoms and the size of the box in nanometers [33].

Parameter Files

In the parameter file (*.mdp) the user can set a range of parameters for their system. The file includes information about e.g. how long you want to run the simulation, time steps (Δt), time constant for coupling, temperature pressure coupling and so on. The parameter file gives Gromacs the data needed to know what to do with the starting structure [33].

Appendix B

Gromacs Programs

This appendix is based on the Gromacs reference manual [35] and the online user guide [11].

Table B.1: Gromacs programs used in MD simulations.

Gromacs program	Description	Output
gmx insert-molecules	Inserts n copies of a molecule into a vacant space or a already existing system. Any velocities present are discarded.	Structure file with added n inserted molecules.
gmx editconf*	Used to rescale the box dimensions of a system.	Re-scaled structure file.
gmx solvate*	Solvates a solute configuration.	Structure file of the now solvated system.
gmx grompp	Reads the topology file, checks the validity of the file, expands the topology from a molecular description to an atomic description.	Creates a binary topology file.
gmx genion	Randomly replaces n solvent molecules with n monoatomic ions.	Structure file with n added monoatomic ions.
gmx mdrun*	Gromacs main computational chemistry engine. Conducts MD simulations, like an energy minimization or an equilibration run of a system under isothermal-isobaric conditions.	A new set of files that describes the newly simulated system.
gmx energy	Extracts energy components from an energy file (.edr) by making the user select which energy component to be studied.	.xvg file (used for plotting graphs) of selected energy configuration and displays averages of the selected energy.
gmx convert-tpr*	Modifies the number of steps in a run input file.	Modified run input file, so the simulation can be extended by further simulation steps
gmx hbond	Computes and analyze hydrogen bonds. Used to count the number of valid hydrogen bonds.	Returns the number of hydrogen bonds over time in a .xvg file.
gmx density	Computes the average density of a substance in the mix.	Returns the average density over time in a .xvg file.
gmx rdf	Calculates radial distribution functions in different.	Returns the RDF over time in a .xvg file.

* The program has more functions than the one described in this table. See [11] for more details.

Appendix C

Gromacs Parameter Files

C.1 TIP4P/2005 and 2,6-Lutidine

C.1.1 Energy Minimization

```
; — Parameters for energy minimization of 2,6-lutidine and water —  
  
; Parameters describing what to do, when to stop and what to save  
integrator = steep ; steep = steepest descent minimization  
entol      = 1.0   ; Stop minimization when the maximum force < 1000.0 kJ/mol/nm  
emstep     = 0.001 ; Energy step size [nm]  
nsteps     = 1000000 ; Maximum number of (minimization) steps to perform  
  
; Output frequency for energies to log file and energy file  
nstlog     = 100  
nstenergy  = 100  
  
; Parameters describing how to find the neighbors and how to calculate the interaction  
ons  
nstlist    = 1 ; Frequency to update of neighbor list and long range forces  
ns_type    = grid ; Method to determine neighbor list (simple, grid)  
rlist      = 1.2 ; Cut-off for making neighbor list [nm]  
coulombtype = cut-off ; Treatment of long range electrostatic static interactions  
rcoulomb   = 1.2 ; Short-range electrostatic cut-off [nm]  
rvdw       = 1.2 ; Short-range Van der Waals cut-off [nm]  
pbc        = xyz ; Periodic Boundary Conditions  
  
vdw-type   = cut-off  
cutoff-scheme = verlet
```

C.1.2 Equilibration Run

```

; — Parameters for equilibration run of 2,6-lutidine and water —

; Run Control parameters
integrator          = md
dt                 = 0.002           ; [ps]
nsteps             = 10000000        ; Maximum number of steps to perform

; Output frequency for coords (x) and velocities (v)
nstxout            = 1000000         ; save coordinates
nstvout            = 1000000         ; save velocities
; Output frequency for energies to log-file and energy-file
nstlog             = 1000000         ; update log file
nstenergy          = 1000000         ; save energies
; Output frequency and precision for xtc-file
nstxtcout          = 1000000         ; Output frequency for xtc file

; Neighborsearching
ns_type            = grid            ; search neighboring grid cells
nstlist            = 10              ; fs
pbc                = xyz             ; 3-D PBC
rlist              = 1.2             ; short-range neighborlist cutoff [nm]
rcoulomb           = 1.2             ; short-range electrostatic cutoff [nm]
rvdw               = 1.2             ; short-range van der Waals cutoff [nm]

; Electrostatics
coulombtype        = PME             ; PME for long-range electrostatics
pme_order          = 4               ; cubic interpolation
fourierspacing     = 0.16           ; grid spacing for FFT
vdw-type           = cut-off

; Coupling
Tcoupl             = Berendsen       ; thermostat
tc-grps            = LUT SOL         ; two coupling groups – more accurate
tau_t              = 0.1 0.1         ; time constant [ps]
ref_t              = 380 380         ; ref. temperature, one for each group [K]
energygrps         = LUT SOL         ; energy groups
Pcoupl             = no              ; no pressure coupling
Pcoupltype         = Isotropic
tau_p              = 1.0
compressibility     = 4.5e-5
ref_p              = 1.0             ; 1 bar

; Generated Velocities
gen_vel            = yes             ; generates velocities
gen_temp           = 380             ; [K]
gen_seed           = -1

; Bonds
constraints         = all-bonds      ; all bonds constrained (fixed length)
continuation        = no
constraint-algorithm = lincs         ; holonomic constraints
lincs_iter          = 1              ; accuracy of LINCS
lincs_order         = 4              ; also related to accuracy

```

C.1.3 Production Run

```

; — Parameters for production run of 2,6-lutidine and water —

; Run Control parameters
integrator          = md
dt                 = 0.002           ; [ps]
nsteps             = 20000000        ; Maximum number of steps to perform

; Output frequency for coords (x) and velocities (v)
nstxout            = 1000000         ; save coordinates
nstvout            = 1000000         ; save velocities
; Output frequency for energies to log-file and energy-file
nstlog             = 1000000         ; update log file
nstenergy          = 1000000         ; save energies
; Output frequency and precision for xtc-file
nstxtcout          = 1000000         ; Output frequency for xtc file

; Neighborsearching
ns_type            = grid           ; search neighboring grid cells
nstlist            = 10              ; [fs]
pbc                = xyz            ; 3-D PBC
rlist              = 1.2             ; short-range neighborlist cutoff [nm]
rcoulomb           = 1.2             ; short-range electrostatic cutoff [nm]
rvdw               = 1.2             ; short-range van der Waals cutoff [nm]

; Electrostatics
coulombtype        = PME             ; PME for long-range electrostatics
pme_order          = 4               ; cubic interpolation
fourierspacing     = 0.16           ; grid spacing for FFT
vdw-type           = cut-off

; Coupling
Tcoupl             = V-rescale       ; thermostat used
tc-grps            = LUT SOL         ; two coupling groups – more accurate
tau_t              = 0.1 0.1        ; time constant [ps]
ref_t              = 380 380         ; ref. temperature, one for each group [K]
energygrps         = LUT SOL         ; energy groups
Pcoupl             = Parrinello-Rahman ; barostat used
Pcoupltype         = Isotropic
tau_p              = 1.0
compressibility     = 4.5e-5
ref_p              = 1.0             ; 1 bar

; Generated Velocities
gen_vel            = no              ; no velocities generates

; Bonds
constraints         = all-bonds      ; all bonds constrained (fixed length)
continuation        = yes
constraint-algorithm = lincs         ; holonomic constraints
lincs_iter          = 1              ; accuracy of LINCS
lincs_order         = 4              ; also related to accuracy

```

C.2 Water/2,6-Lutidine Mixture with Salt

C.2.1 Energy Minimization

```
; — Parameters for energy minimization of water/2,6-lutidine and PPh4Cl —
; Parameters describing what to do, when to stop and what to save
integrator = steep ; steep = steepest descent minimization
emtol = 1.0 ; Stop minimization when the maximum force < 1000.0 kJ/mol/nm
emstep = 0.001 ; Energy step size [nm]
nsteps = 1000000 ; Maximum number of (minimization) steps to perform

; Output frequency for energies to log file and energy file
nstlog = 100
nstenergy = 100

; Parameters describing how to find the neighbors and how to calculate the interactions
nstlist = 10 ; Frequency to update of neighbor list and long range forces
ns_type = grid ; Method to determine neighbor list (simple, grid)
rlist = 1.2 ; Cut-off for making neighbor list [nm]
coulombtype = PME ; Treatment of long range electrostatic interactions
rcoulomb = 1.2 ; Short-range electrostatic cut-off [nm]
rvdw = 1.2 ; Short-range Van der Waals cut-off [nm]
pbc = xyz ; Periodic Boundary Conditions

vdw-type = cut-off
```

C.2.2 Equilibration Run

; — Parameters for equilibration run of water/2,6-lutidine and PPh4Cl —

```
; Run Control parameters
integrator          = md
dt                 = 0.002           ; [ps]
nsteps             = 10000000        ; Maximum number of steps to perform

; Output frequency for coords (x) and velocities (v)
nstxout            = 1000000        ; save coordinates
nstvout            = 1000000        ; save velocities
; Output frequency for energies to log-file and energy-file
nstlog             = 1000000        ; update log file
nstenergy          = 1000000        ; save energies
; Output frequency and precision for xtc-file
nstxtcout          = 1000000        ; Output frequency for xtc file

Neighborsearching
ns_type            = grid           ; search neighboring grid cells
nstlist            = 10             ; fs
pbc                = xyz            ; 3-D PBC
rlist              = 1.2            ; short-range neighborlist cutoff [nm]
rcoulomb           = 1.2            ; short-range electrostatic cutoff [nm]
rvdw               = 1.2            ; short-range van der Waals cutoff [nm]

; Electrostatics
coulombtype        = PME            ; PME for long-range electrostatics
pme_order          = 4              ; cubic interpolation
fourierspacing     = 0.16          ; grid spacing for FFT
vdw-type           = cut-off

; Coupling
Tcoupl             = Berendsen      ; thermostat
tc-grps            = LUT SOL CL_WEO ; one coupling per group
tau_t              = 0.1 0.1 0.1 0.1 ; time constant, in ps
ref_t              = 380 380 380 380 ; ref. T, one for each group [K]
energygrps         = LUT SOL CL_WEO
Pcoupl             = no             ; no pressure coupling
Pcoupltype         = Isotropic
tau_p              = 1.0
compressibility     = 4.5e-5
ref_p              = 1.0            ; 1 bar

; Generated Velocities
gen_vel            = yes            ; generates velocities
gen_temp           = 380            ; [K]
gen_seed           = 712349

; Bonds
constraints         = all-bonds     ; all bonds constrained (fixed length)
continuation        = no
constraint-algorithm = lincs        ; holonomic constraints
lincs_iter          = 1              ; accuracy of LINCS
lincs_order         = 4              ; also related to accuracy
```

C.2.3 Production Run

```

; — Parameters for production run of water/2,6-lutidine and PPh4Cl —

; Run Control parameters
integrator          = md
dt                  = 0.002           ; [ps]
nsteps              = 200000000       ; Maximum number of steps to perform

; Output frequency for coords (x) and velocities (v)
nstxout             = 1000000         ; save coordinates
nstvout             = 1000000         ; save velocities
; Output frequency for energies to log-file and energy-file
nstlog              = 1000000         ; update log file
nstenergy           = 1000000         ; save energies
; Output frequency and precision for xtc-file
nstxtcout           = 1000000         ; Output frequency for xtc file

Neighborsearching
ns_type             = grid            ; search neighboring grid cells
nstlist             = 10              ; fs
pbc                 = xyz             ; 3-D PBC
rlist               = 1.2             ; short-range neighborlist cutoff [nm]
rcoulomb            = 1.2             ; short-range electrostatic cutoff [nm]
rvdw                = 1.2             ; short-range van der Waals cutoff [nm]

; Electrostatics
coulombtype         = PME             ; PME for long-range electrostatics
pme_order           = 4               ; cubic interpolation
fourierspacing      = 0.16           ; grid spacing for FFT
vdw-type            = cut-off

; Coupling
Tcoupl              = V-rescale       ; thermostat
tc-grps             = LUT SOL CL_WEO  ; one coupling per group
tau_t               = 0.1 0.1 0.1 0.1 ; time constant, in ps
ref_t               = 380 380 380 380 ; ref. T, one for each group [K]
energygrps          = LUT SOL CL_WEO
Pcoupl              = Parrinello-Rahman ; barostat (Berendsen for interfacial ten.)
Pcoupltype          = Isotropic
tau_p               = 1.0
compressibility      = 4.5e-5
ref_p               = 1.0             ; 1 bar

; Generated Velocities
gen_vel             = no              ; no velocities generates

; Bonds
constraints         = all-bonds       ; all bonds constrained (fixed length)
continuation         = yes
constraint-algorithm = lincs          ; holonomic constraints
lincs_iter           = 1              ; accuracy of LINCS
lincs_order          = 4              ; also related to accuracy

```